B. Attal-Trétout
F. Grisch
D. Packan
I. Ribet-Mohamed
M. Lefebvre
(Onera)

E-mail: brigitte.attal-tretout@onera.fr

Laser Spectroscopy for in Situ Diagnostics

Laser spectroscopy based on nonlinear processes such as four wave mixing and laser-induced gratings or based on spontaneous Raman and Thomson scattering is widely used, from near IR to near UV, to probe reactive media. The bulk of this monograph is devoted to the application of these techniques to the specific area of plasma, combustion and hypersonic flow field. For each technique a brief description of the signal amplitude is given from which spectral and/or temporal evolution can be predicted as a function of temperature and pressure. Experimentally, the dependence of the signal on parameters such as temperature, pressure, gas composition, or the energy of pump and probe laser pulses have been investigated. Comparison of the experimental results with theoretical predictions allows us to accurately measure these parameters in situ. Therefore, temperature, velocity or number density of important species (major or minor) can be derived from the spectral or temporal content. The synchronization of pulsed laser with particular physical phenomena provides time evolution of the sample over a μs or ms duration, depending on the probed events, thanks to the time resolution (ns) of the lasers. Several examples are given. CARS is applied to a buoyant H_2/air flame, a monodisperse droplet stream in combustion and a pulsed plasma in a methane/air flow. In each case, time and space evolution of temperature is recorded. DFWM has proved particularly useful for probing NO, especially when spectral interference is overwhelming the LIF signal; LIF is used otherwise. Laser induced gratings are also valuable tools in some typical cases. Examples are given to illustrate their potential in measuring NO_2 molecules in a flame and in measuring the temperature and velocity of a high speed flow. Finally, electron density can be inferred using Thomson scattering and an application in the pulsed plasma is presented.

Introduction

Over the past decades a great deal of researches were devoted to the development of diagnostic methods for environments that are particularly difficult to analyze, like turbulent flames, hypersonic flows or plasmas. Indeed, only non invasive techniques that are able to measure simultaneously temperature, density and velocity are suitable to fully characterise combustion reactive flows or non-equilibrium flows. At Onera, non-equilibrium flows are produced in high enthalpy wind tunnels. We have dedicated the paper to typical cases such as the processes of energy transfer between a plasma and gas medium, between flame and vortices and also inside two-phase combustion. They yet represent a key issue to improve the understanding of the main mechanisms taking place in a discharge-flame or flame-vortex or flame-droplet interaction. The main objective of the present work is to investigate the thermodynamics and kinetic properties of these reactive media through optical diagnostics, on a fundamental basis as well as for application to practical systems [26].
In this context, experimental values of the population distributions of neutral molecules are important quantities which can be used as input parameters for the simulation of these interactions. Due to the specifications of the pulsed events such as limited spatial dimensions and short duration, only laser-based methods have the potential to provide information without disturbing the media. The development of pulsed laser of large power initiated the research in diagnostic techniques which are today always providing more data in shorter duration and on larger scale. The more elaborate are the technology of lasers and detectors and the more efficient are the measurements. Laser techniques have high spatial and temporal resolution, enabling locally and temporally resolved measurements of temperature and species concentration. Among the various diagnostics techniques, non linear techniques provide stronger and collimated signals allowing highly luminous media at high temperature and pressure to be studied in situ [1,2]. Among other, coherent anti-Stokes Raman scattering (CARS) was developed at Onera and extensively used for temperature measurements in hostile reactive environments presenting interest in the aeronautic field. The basic principle of temperature measurements by CARS is to probe relative population of the molecular levels from

which the thermodynamic temperature of the molecular system is drawn. Then, a peculiar objective of our work was to combine techniques to retrieve more data simultaneously.

First, we discuss the principle of the CARS and DFWM laser techniques and give some examples of measurements targeting the temporal sampling of repetitive events. The thermal gratings are then presented; they are applied to the probing of NO_2 in ambient air and flames. In that section, electrostrictive gratings are also combined with CARS to obtain the speed of the flow and the temperature respectively, in a wind tunnel. Thomson scattering, applied to a pulsed plasma investigation is presented in Box 1.

Laser-based techniques

Four wave mixing processes: CARS, DFWM

Third order processes are the strongest non linear processes in centrosymetric media and form the basis for Doppler free polarization spectroscopy, Doppler free two photon absorption, Stimulated Raman gain spectroscopy (SRS), inverse Raman scattering (IRS), Coherent stokes Raman scattering (CSRS), Degenerate four wave mixing (DFWM) and Coherent anti-Stokes Raman Scattering (CARS). CARS, which was first observed by Maker and Terhune [3] is but one of many well-known third order processes. CARS offers many advantages over conventional Raman techniques since very intense signals can be detected in most of the major species. These advantages are inherent to its coherent nature, leading to collimated emission and efficient detection of the anti-Stokes signal. It has been used successfully for single point, single shot temperature measurement in a variety of combustion, low pressures gases, discharges and plasmas. The "resonance enhanced" CARS technique (RECARS) applies more particularly to the probing of trace species and a degenerate version of the four wave mixing process called DFWM [4] offer a simpler alternative to RECARS offering similar detectivity [5,6]. In the resonant process, the incident laser frequencies are tuned to reach one photon transitions of the molecules.

Model description

CARS takes place in media with a Raman active vibrational modes (ω_v). It is observed when two collinear beams of frequencies ω_1 (laser) and ω_2 (Stokes) such that $\omega_1 - \omega_2 = \omega_v$ are passed through the sample (Figure 1). A new wave is generated at the anti-stokes frequency $\omega_3 = 2\omega_1 - \omega_2$ in the forward direction and collinear with the exciting beams (Figure 2a). The new wave is often described as resulting from the inelastic scattering of the wave "ω_1" by the molecular vibrations (coherently driven by the incident waves at ω_1 and ω_2). We note that the same mechanism creates, in the degenerate case (DFWM), a similar wave at $\omega = \omega_4 = \omega_1 = \omega_2 = \omega_3$ (Figure 2b). If the incident beams have different polarizations, these states of polarization are changed by the interaction and this property is also used to improve the nonlinear background rejection in CARS and to improve the laser light rejection in DFWM [7, 8] (Figure 2c). CARS spectroscopy is performed with a fixed ω_1 frequency and by tuning the frequency ω_2 in order to scan the Raman resonance. Broadband multiplex CARS is an interesting excitation scheme using a broad width Stokes (60 to 80 cm^{-1}) from which temperature can be measured instantaneously, since the whole anti-Stokes spectra is recorded in a single shot on a ICCD camera (Figure 1 b).

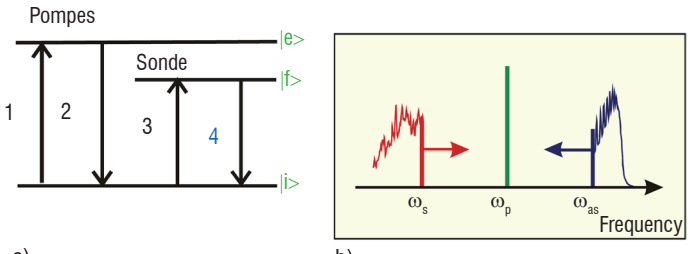

a) b)

Figure 1 - (a): Energy level scheme of a four wave mixing process; 1,2,3,and 4 are the four steps of the process; (b): excitation scheme of the multiplex CARS; ω_p, ω_s and ω_{as} are the frequencies of the laser, Stokes and anti-Stokes beams. $\omega_1 = \omega_3 = \omega_p$; $\omega_s = \omega_2$; $\omega_4 = \omega_{as}$

The intensity variation of the new wave created at ω_3 (or ω) is driven by the induced third order non linear polarization ω (ω_3). The spectral features are representative of the squared modulus of the third order non linear susceptibility ω_3 (ω_3) according to the following formulae:

$$P(\omega_3) = 4\omega_3^4 / c^4 \left| X^{(3)}(-\omega_3, \omega_1, \omega_1, -\omega_2) \right|^2 P_1^2 P_2 \text{ in CARS,}$$

$$P(\omega) = 4\omega^4 / c^4 \left| X^{(3)}(-\omega, \omega, \omega, -\omega) \right|^2 P^3 \text{ in DFWM,}$$

where P_1 (P) and P_2 are the power of the incident beam at ω_1 (ω) and ω_2 respectively.

This expression is valid assuming that the signal is generated using focused laser beams, in a small cylindrical volume around the focus of the beams. Its length is equal to the confocal parameter 1 of the

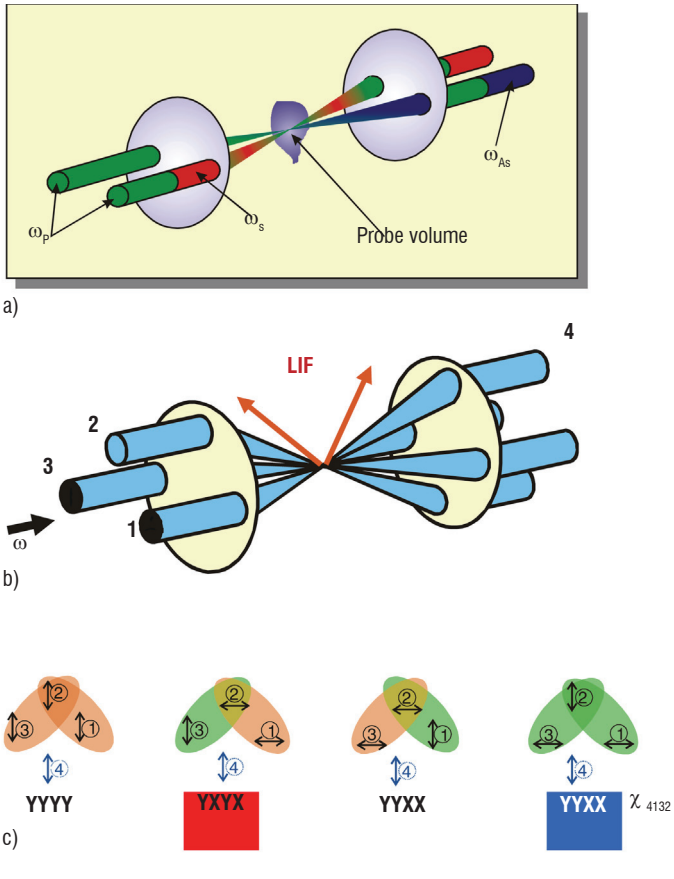

Figure 2: (a): BOXCARS geometry of the CARS excitation; (b): folded BOX-CARS geometry applied to DFWM; (c): polarisation arrangement used in four wave mixing processes with the corresponding susceptibility χ_{4132}; laser induced fluorescence (LIF) signal, which is incoherent, is emitted in 4π steradian.

beams with $1 = \pi\Phi^2 / 2\lambda$ and for Gaussian beam the waist at the focus is $\Phi = 4\lambda f / \pi d$ where f is the focal length of the lens and d the incident laser beam diameter in the plane of the lens.

At triple resonance, a strong increase of the nonlinear susceptibility is observed relatively to the non resonant background which greatly improves the contrast of the lines since all transitions become resonant together (see equation (1)). Thanks to that property, resonance CARS (RECARS) and DFWM were successfully applied to most of the radicals of interest in physical chemistry using tunable dye lasers. Detectivity threshold can reach 10^{11} cm^{-3} at one bar total pressure on resonance [5,9] whereas conventional CARS is usually detected on major species (typically $>10^{16}$ cm^{-3}) [2].
Using density matrix formalism, the resonant susceptibility of CARS is derived using a perturbative treatment of the field interaction which gives [9]:

$$e_4 X^{(3)}\left(-\omega_3,\omega_1,\omega_1,-\omega_2\right)e_1 e_3 e_2 = N/\hbar^3 \sum_{a,b,n,n'} \mu_{an'}^{(4)} \mu_{n'b}^{(3)} \mu_{bn}^{(2)} \mu_{na}^{(1)}$$
$$\int \left(A_1 - B_1 + B_2 - B_3\right) F\left(v_z\right) dv_z \qquad (1)$$

with :

$$A_1 = \rho_{aa}^{(0)}\left[\left(\omega_{na} - \omega_1 + k_1.v_z - i\Gamma_{na}\right)\times \left(\omega_{ba} - \omega_1 + \omega_2 + \left(k_1 - k_2\right)v_z - i\Gamma_{ba}\right)\times \left(\omega_{n'a} - \omega_4 + k_4.v_z - i\Gamma_{n'a}\right)\right]^{-1}$$

$$B_1 = \rho_{bb}^{(0)}\left[\left(\omega_{nb} - \omega_2 + k_2.v_z + i\Gamma_{nb}\right)\times \left(\omega_{ba} - \omega_1 + \omega_2 + \left(k_1 - k_2\right)v_z - i\Gamma_{ba}\right)\times \left(\omega_{n'a} - \omega_4 + k_4.v_z - i\Gamma_{n'a}\right)\right]^{-1}$$

$$B_2 = \rho_{bb}^{(0)}\left[\left(\omega_{n'b} - \omega_3 + k_3.v_z - i\Gamma_{n'b}\right)\times \left(\omega_{n'n} - \omega_3 + \omega_2 + \left(k_3 - k_2\right)v_z - i\Gamma_{n'n}\right)\times \left(\omega_{n'a} - \omega_4 + k_4.v_z - i\Gamma_{n'a}\right)\right]^{-1}$$

$$B_3 = \rho_{bb}^{(0)}\left[\left(\omega_{nb} - \omega_2 + k_2.v_z + i\Gamma_{nb}\right)\times \left(\omega_{n'n} - \omega_3 + \omega_2 + \left(k_3 - k_2\right)v_z - i\Gamma_{n'n}\right)\times \left(\omega_{n'a} - \omega_4 + k_4.v_z - i\Gamma_{n'a}\right)\right]^{-1}$$

where $\mu_{\alpha\beta}^{(i)} = -\mu_{\alpha\beta}.e_i$ and $\alpha\beta = a,b,n,n'$; $N\rho_{\alpha\alpha}^{(0)}$ is the population of the molecular level $|\alpha>$ and N is the total number density.
One has in forward DFWM [4,6,7]:

$$X^{(3)}\left(-\omega,\omega,\omega,-\omega\right) = N B_{an}^2\left[\rho_{aa}^{(0)} - \rho_{nn}^{(0)}\left(2J_a + 1/2J_n + 1\right)\right]$$
$$L\left(\omega\right)G_F^T\left(e_4,e_1,e_3,e_2,J_a,J_n,\omega\right) \qquad (2)$$

with $L(\omega) = L_{12}^a\left(\omega\right) + L_{32}^a\left(\omega\right) + L_{12}^n\left(\omega\right) + L_{32}^n\left(\omega\right)$ where $L_{j2}^{\alpha}(\omega)$ is a complex line shape function defined by :

$$L_{j2}^{\alpha}(\omega) = \int\left[\left(\omega_{na} - \omega + k_j.v_z - i\Gamma_{na}\right)^{-1} - \left(\omega_{na} - \omega + k_2.v_z + i\Gamma_{na}\right)^{-1}\right]\times \left(\omega_{na} - \omega + k_4.v_z - i\Gamma_{na}\right)^{-1} F(v_z)\,dv_z \Big/ \left[\left(k_j - k_2\right)v_z - i\Gamma_{\alpha}\right]$$

and $(j = 1,3)$.
Also one has:

$$G_F^T\left(e_4,e_1,e_3,e_2,J_a,J_n,\omega\right) = W_{13}(\omega)\,G_F\left(e_4,e_1,e_3,e_2,J_a,J_n\right) + W_{31}(\omega)\,G_F\left(e_4,e_3,e_1,e_2,J_a,J_n\right)$$

$G_F\left(e_4,e_3,e_1,e_2,J_a,J_n\right)$ are the geometrical factors that depends solely on the polarisation unit vectors e_i and on the total angular momentum quantum numbers J_a and J_n [7,8]. W are weighting factors defined by

$$W_{13}(\omega) = \left[L_{12}^a(\omega) + L_{32}^n(\omega)\right] / L(\omega)$$
$$W_{31}(\omega) = \left[L_{32}^a(\omega) + L_{12}^n(\omega)\right] / L(\omega)$$

The strength of the electronic transition moment $\mu_{\alpha\beta}$ of the resonant step (or the Einstein coefficient $B_{\alpha\beta}$) is driving the electronic enhancement and the final intensity of the signal in RECARS and DFWM. As a matter of fact, much larger signals are observed in atomic species such as Iron or Cesium than in radicals such as OH or CH and signals are even smaller in tri atomic such as NH_2. Moreover, a precise set of spectroscopic data must be available to correctly interpret the CARS and DFWM spectral content [4,9]. Finally, to measure a concentration, signal dependence versus spectroscopic parameters and temperature must be known in order to retrieve the number density N from the signal amplitude. Optical diagnostics accurately provides relative concentration but absolute values are only measured through calibration of the signal at normal temperature and pressure.

Temporal resolution

CARS was also developed with femtosecond pulses to study reaction dynamics and to take advantage from the good stability of the laser power and the high repetition rates of these lasers [10]. However, spectroscopy of gases is straightforward and was first applied using spectral resolution in the 0,1 to 1 cm^{-1} range easily achieved with nanosecond laser sources. A disadvantage of the femtosecond regime in gases is the rise of the peak power density which produces much stronger saturation effects [8]. In nonlinear processes, the detectivity limit of diagnostic techniques is usually limited by these effects when laser power is increased in order to reach optimum sensitivity. The stationary regime is also changed since the stationary approximation is not valid anymore when the state lifetime becomes larger than the laser duration. Transient solutions of the system evolution have to be calculated.
At Onera, much of the effort was dedicated to the probing of atoms and molecules using nanosecond laser sources, some of which are presented in the following. The sampling of the reactive media using nanosecond pulses allow us to investigate the space and time evolution of temperature and concentrations during periodic events such as vortex flames or plasma generated by a periodic discharge. These experiments are presented in section 2-1-4. The sequence of event displayed in figure 3 is used thanks to a simple synchronization of the laser with the flame (or plasma) period and with the gate of the detector (ICCD camera or PM tube).

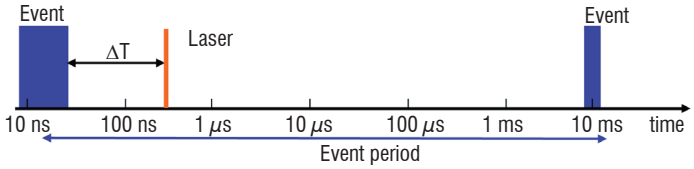

Figure 3 - Sequence of analysis of a short time event by a pulsed laser.

Figure 4 - CARS image of polystyrene balls of 3 μm in diameter.

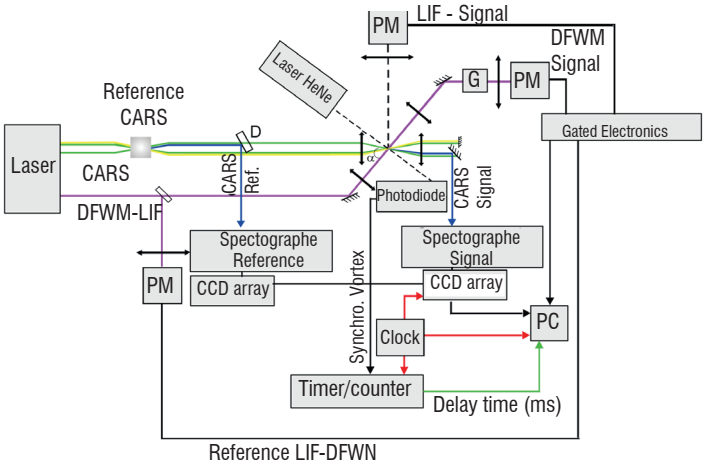

Figure 5 - Experimental set up combining CARS, DFWM and LIF techniques.

a)

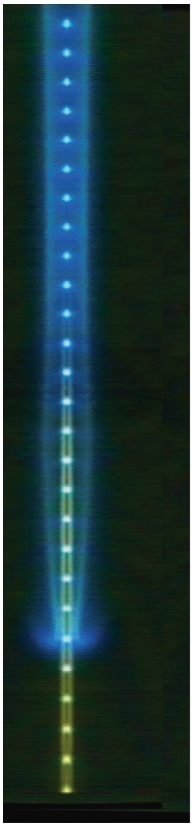

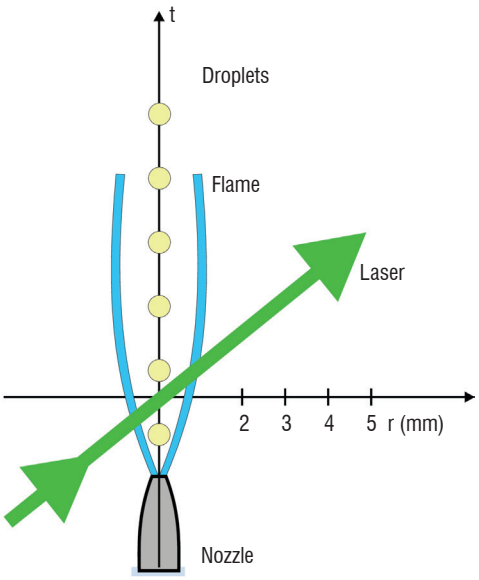

Figure 7 - View of the burning monodispersed droplet stream.

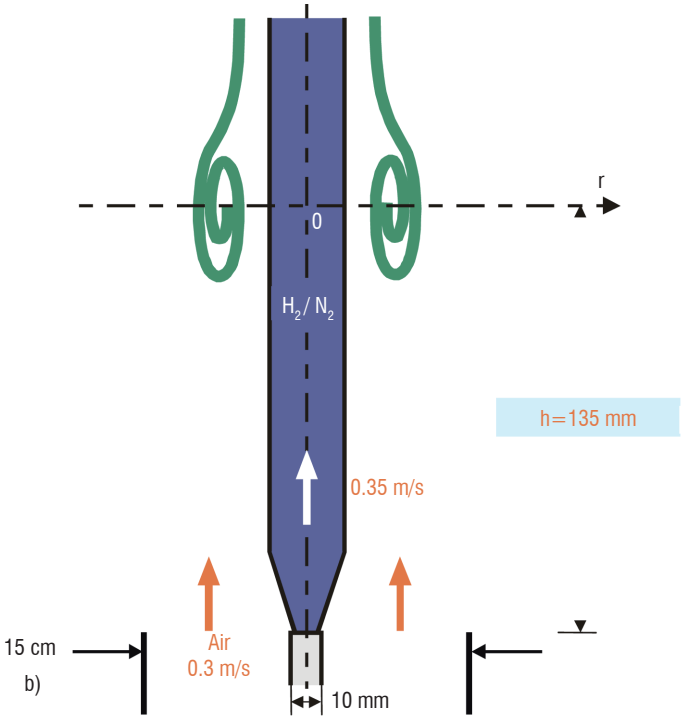

b)

Figure 6 - Buoyant H_2/air flame, producing vortices at a period of 15Hz, (a): flame; (b):scheme.

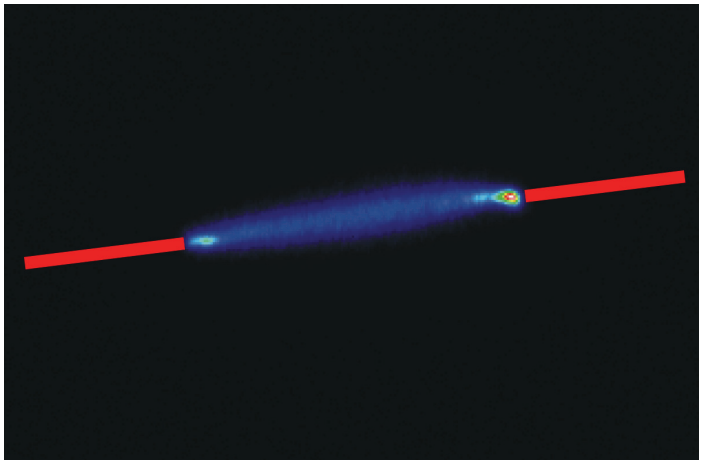

Figure 8 - Pulsed plasma generated by a 20 kV, 70 ns discharge.

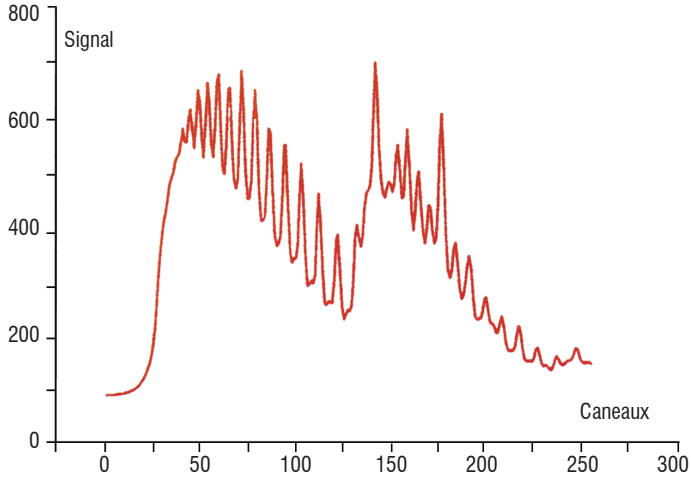

Figure 9 - N_2 CAR-S spectrum obtained in a flame using multiplex CARS , the Stokes is 100 cm^{-1} wide and the laser power is about 30 mJ for P1 and 5 mJ for P2.

Spatial resolution

It was shown that 75 % of the anti-Stokes power is generated within a length lr= 61 which is defined as the spatial resolution. The expression (1) is valid as long as lr is smaller than the coherence length lc. The coherence length depends of the dispersion of the media and is much shorter in liquids and solid than in gases. In gases, the spatial resolution lr is about 8 mm for d=3 mm and f=10 cm, therefore another arrangement is used providing a better resolution called BOXCARS geometry. By splitting the pump at ω_1 into two parallel beams, the signal is created in the focal volume common to all three incident beams, and can be reduced to less than 1 mm (figure 2) At macroscopic scale, the focusing geometry only allows nonlinear techniques to provide a single point, single shot information. The sample volume is a small cylinder of 100 μm in diameter and 1 mm in length. One main advantage of LIF is that imaging is simple to implement by using laser sheets whereas mainly single point measurements are presented in the following sections [27].
However, during the last decade, CARS has been also developed in near field microscopy thus providing images at the focus of the microscope which are usually few tens of μm in size (Figure 4) with a spatial resolution which can reach less than one μm [11].

The Probing of mixtures

The analysis of gas mixtures has motivated most of the work performed so far. Conventional CARS is then mainly used to measure the gas temperature while DFWM or LIF is used to measure transient species concentration. The coupling of CARS thermometry with DFWM and LIF method is achieved thanks to a set up built by SOPRA (Figure 5). The laser system was especially designed to allow simultaneous trace species analysis and conventional CARS thermometry. Determination of NO concentrations is presented in the flames experiments (Figure 6 and 7) whereas major species like H_2, CH_4 and C_2H_2 are sampled in the plasma experiment (Figure 8).
Two benches are mounted on a single table in order to deliver the pump and Stokes beams required for the multiplex CARS temperature measurement and the UV beam necessary to monitor the NO concentration. The first bench comprises a frequency doubled injection seeded Nd: YAG laser and a broad band dye laser that generates the CARS signal of nitrogen Raman Q branches (Figure 9). The second laser bench consists of a suitable narrow-band dye laser pumped by a multi mode Nd: YAG laser which is frequency doubled in a BBO crystal to generate the UV beam at 226 nm. The output energy is about 3 mJ per pulse with FWHM of 0.12 cm^{-1}. The laser repetition rate is 10 Hz width 10 ns and the two laser systems are synchronized within the temporal jitter (1 or 2 ns). The CARS and UV beams are focused co-linearly using respectively 300 mm and 900 mm focal length lens. The hole is drilled at the centre of the 300 mm lens in order to allow the UV beams to be focused at the same point on the CARS beams. A BOXCARS geometry is used for the CARS beams (Figure 2a): refocusing and non-resonant background cancellation is applied systematically. This geometry provides a 3 mm long, 80 μm diameter CARS probe volume superimposed on a 1 mm long, 150 μm diameter UV probe volume. The long UV focal length is used to prevent saturation of the NO transition in the $A^2\Sigma - X^2\pi\,(0-0)$ γ system (Figure 10). The superposition of the CARS and DFWM/LIF probe volume is performed using a pinhole mounted on three translation stage and positioned carefully to allow beam superposition with an accuracy of about ± 20 μm. Reference and sample CARS spectra are dispersed in separate spectrometers and detected by means of diode arrays. The DFWM and LIF signals are detected by Photo Multiplier Tubes (PMT). In LIF, spectral filtering of the NO line is used, namely the Q1(21,5) in the (0-0) band of the γ system.

Buoyant H_2/air flame

In order to illustrate the great potential of these non linear optical techniques, we show the results of the study of a buoyant H_2/air flame for which instantaneous measurements in a periodically oscillating jet diffusion flame (Figure 6) were obtained [12], [26]. The temporal and spatial evolutions of the vortex/flame interactions were investigated by phase-locking the measurements and using laser diagnostics in combination. CARS was used to measure temperature, and DFWM and LIF were used for the concentrations of NO and radicals. Synchronisation is achieved by using the following procedure: the frequency of the outer vortices was monitored by passing a He-Ne laser beam through the outer part of the flame and detecting the beam wandering using a PIN photodiode. The phase angles at which single-shot measurements were performed were obtained by measuring the delay between the laser pulses and the periodic signal generated by the PIN photodiode using a counter/timer (Hewlett-Packard). Point measurements were made in the flame by translating the burner to the specified axial (z) and radial (r) locations. The radial position was changed in coarse steps of 1 mm. For each location single-point measurements were recorded in real-time over several successive

cycles of the buoyant vortices. Typically, sequences of 500 laser shots were recorded with a laser repetition rate of 9.8 Hz to obtain a sampling time of ~ 1 ms.

Temperature (K)	NO_2 detectivity (ppm)
670	5
775	22
830	63

Table 1 - Estimated NO_2 detectivity in the CH_4/air flame.

Temperature (K)	NO_2 detectivity (ppm)
520	9
640	12
760	17

Table 2 - Estimated NO_2 detectivity in the H_2/air flame.

Variations in temperature and NO concentrations were recorded simultaneously as a function of time over a vortex-crossing period at different locations in the flame. For validating the theoretical model, a location with axial and radial distances of 135 and 15.5 mm, respectively, was chosen. As the vortices travel past this probe location, hot combustion products convect not only in the axial direction but also in the radial direction. Typical time-dependent profiles of measured temperature and [NO] at this location are shown in Figure 11 with solid circles and squares, respectively. These profiles represent the data in the bulge region during the vortex-flame interaction. The two peaks in temperature-time plot (Figure 11) are highly reproducible and represent stretched and compressed flamelets [12]. When the flame is bulged in the braid region of a vortex pair, the flame section (flamelet) that is being pulled outward by the lower vortex becomes compressed, and the flame section being pushed inward by the upper vortex becomes stretched. This means, with reference to time that the flame section crossing the probe location first (t ~ 13 ms) represents the stretched flame (due to the upper vortex) and the one crossing later (t ~ 30 ms) represents the compressed flame (due to the lower vortex).

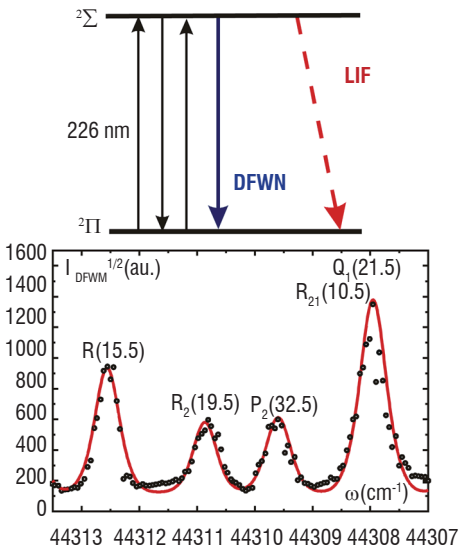

Figure 10 - NO excitation scheme in DFWM and corresponding spectrum recorded at resonance in the γ system in a flame at 2000K and 1bar.

Contour plots of the measured parameters in space and time were constructed from the individual time profiles recorded at several radial locations (Figure 12). About 10 single-shot measurements were averaged at each temporal (phase) and spatial position, i.e., at a specified height (135 mm from the burner) and a specified radius (1-mm intervals from the center), about 10 measurements were made every 1 ms during the flame-flicker period (~ 65 ms) and averaged to obtain one value in the contour map. Experimentally, it was observed that islands of high-temperature (Figure 12a) and high [NO] (Figure 12b) developed in the compressed region of the flame bulge (~ 40 ms). It is interesting to note that the location of the NO peak was shifted slightly by a few millimeters in the radial direction from that of the peak temperature. In the stretched region of the flame, measurements also showed a peak-temperature drop of ~ 100 K, which is consistent with the simulations (Figure 12c). [NO] followed the temperature, with the peak located in the bulge region, as predicted in the calculations (Figure 12 d). Finally, [NO] closely follows the temperature, with the peak in the former being located in the bulge region. The large [NO] in the compressed flame arises, in part, from the transport of the NO generated in other regions of the flame.

Monodisperse droplet stream in combustion

These techniques can also be applied to the study of multiphasic media, such as droplets combustion. We use a droplet injector which has a 50 μm internal diameter orifice to generate the ethanol droplet stream (Figure 7a) probed by the CARS and LIF laser beams. The laser beams are focussed at 20 mm above the injector (Figure 7b) and the droplet size is about 100 μm in the configuration under study [28].

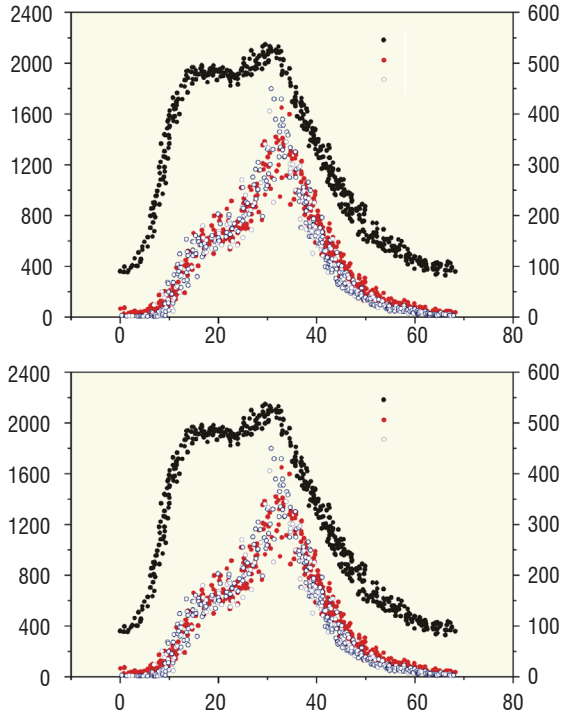

Figure 11 - Temporal evolution of the temperature and NO concentration obtained by CARS and by DFWM and LIF respectively ; (a): in the centre of the vortex, (b): on the edge of the vortex.

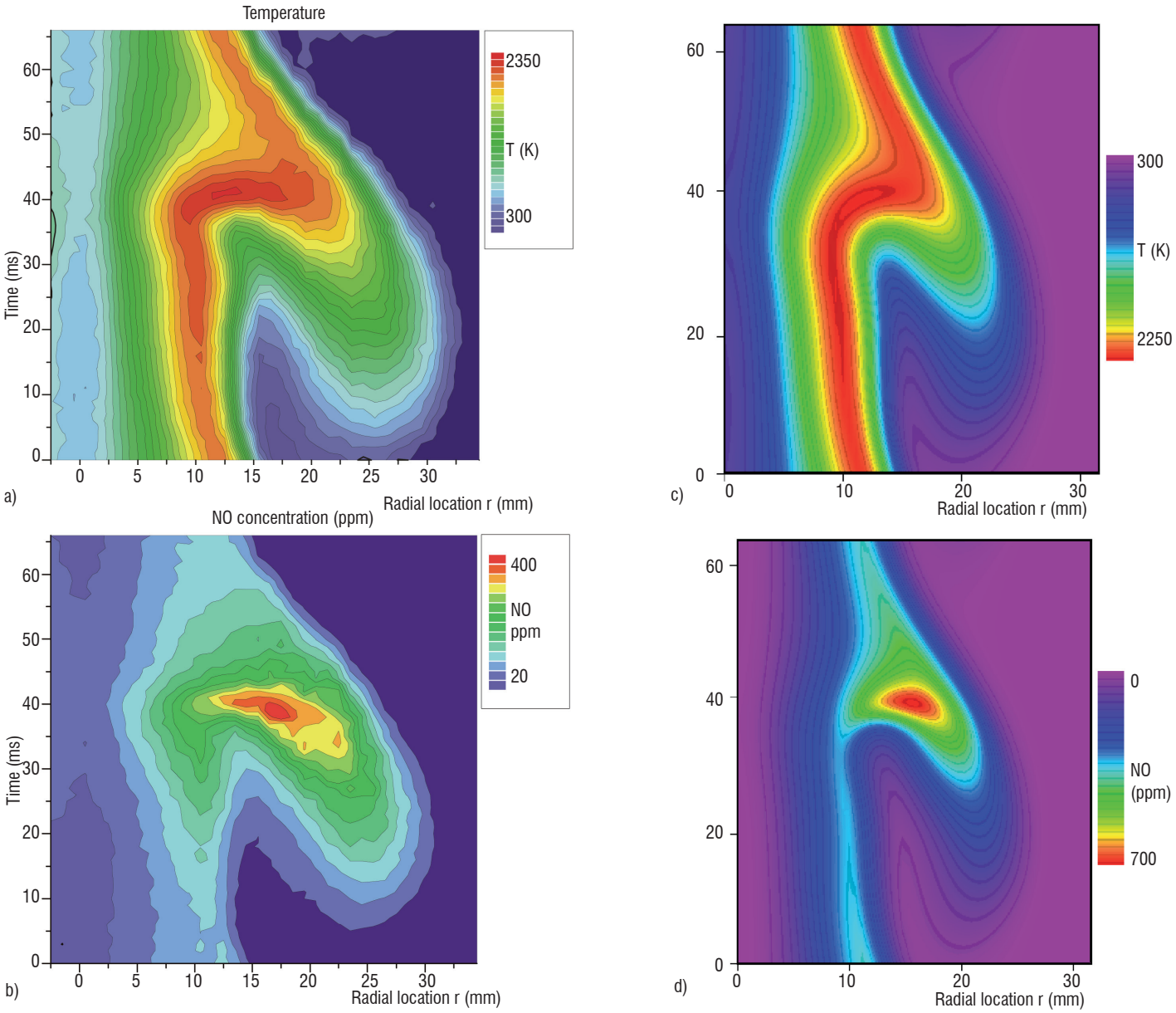

Figure 12 - Measured two dimensional map of temperature (a) and NO concentration (b) in the vortex flame and corresponding calculation of [12] for T (c) and NO (d).

Two excitation frequencies are used experimentally, 16700 and 33200 Hz, which correspond to a droplet spacing parameter C=6 and 3 respectively [13]. A careful check of the datation system is performed prior to the sequence of measurements. Sets of 400 single shots are acquired and plotted as a function of time over a period of 60 μs (30μs) for the 16700 Hz (33200 Hz) generator frequency. Instantaneous measurements are regularly spread over the period with about 6 points in each μs range. The flame radius is scanned over 20 successive positions to sweep the flame in which the reaction zone is located at about 1.6 mm from the droplet axis (Figure 7b). Time profiles are presented over a droplet period in figure 13. The region located between the droplet axis and the flame zone is displayed in figure 13a and the region located beyond the reaction zone is shown in figure 13b. The droplet is easily seen in figure 13a since optical breakdown occurs when the laser beams are focussed inside the droplets. In this case the acquisition routine automatically rejects the measurements. Averaged profiles further illustrate the temperature and NO concentration evolution along the flame radius (Figure 14).
On the logarithmic scale of figure 14, the UV signal rapidly change near the flame centre where the signal strength is already two orders of magnitude smaller than at the droplet axis. In the flame, NO signal becomes predominant and then smoothly decreases toward the burnt gas region. The slow decrease is suggesting that thermal NO is mainly produced according to the drop in temperature also measured in that region (Figure 14). The first observation is due to the laminar character of that kind of flame. However, the spatial resolution can degrades the temperature sampling within the accuracy of 50 K given by standard deviation and the steady state nature of the temperature profile may not be unambiguously demonstrated everywhere above the nozzle. The second observation is related to the strength of the UV signal on the droplet axis suggesting that other species may be at the origin of that signal. Consequently, the spectral discrimination of the NO signal was performed by setting the laser frequency to the top of the Q1(21.5) line whereas parasite UV contribution is measured by shifting the frequency in the wing of the NO line. In figure 15, the radial appearance of NO at the flame centre is demonstrated whereas important background is observed between 0 and 1.2 mm radial location.

The time behaviour of temperature and NO is found flat whatever the flame conditions investigated (16700 Hz and 33200 Hz). The steady state character of the temperature profile is representative of a laminar diffusion flame which is obtained at 20 mm above the nozzle. The steady state regime is probably not fully achieved near the nozzle orifice for the first droplets of the stream [13]. The temperature maximum is 2160K (within the 50 K accuracy) and corresponds to the equilibrium temperature of stoechiometric ethanol/air combustion. In the two flame investigated, that value does not versus height above the nozzle. The location of the flame front is constant, at r= 16 mm in the two flames. The NO concentration peaks in the flame zone and its concentration reaches 100 ppm at 33200Hz and 70 ppm at 16700Hz as shown in figure 14. The closer the droplets, the lower is the burning rate therefore leading to a higher NO concentration. It is known that the closer the droplets are, the less is the evaporating rate. Actually, the vapor liberated by a front droplet surrounds the following droplet because their spacing parameter is small. As a result, the following droplet has a lower evaporating rate due to the vapor saturated environment. The change in NO production is thus related to the flame condition through the change in spacing parameter.

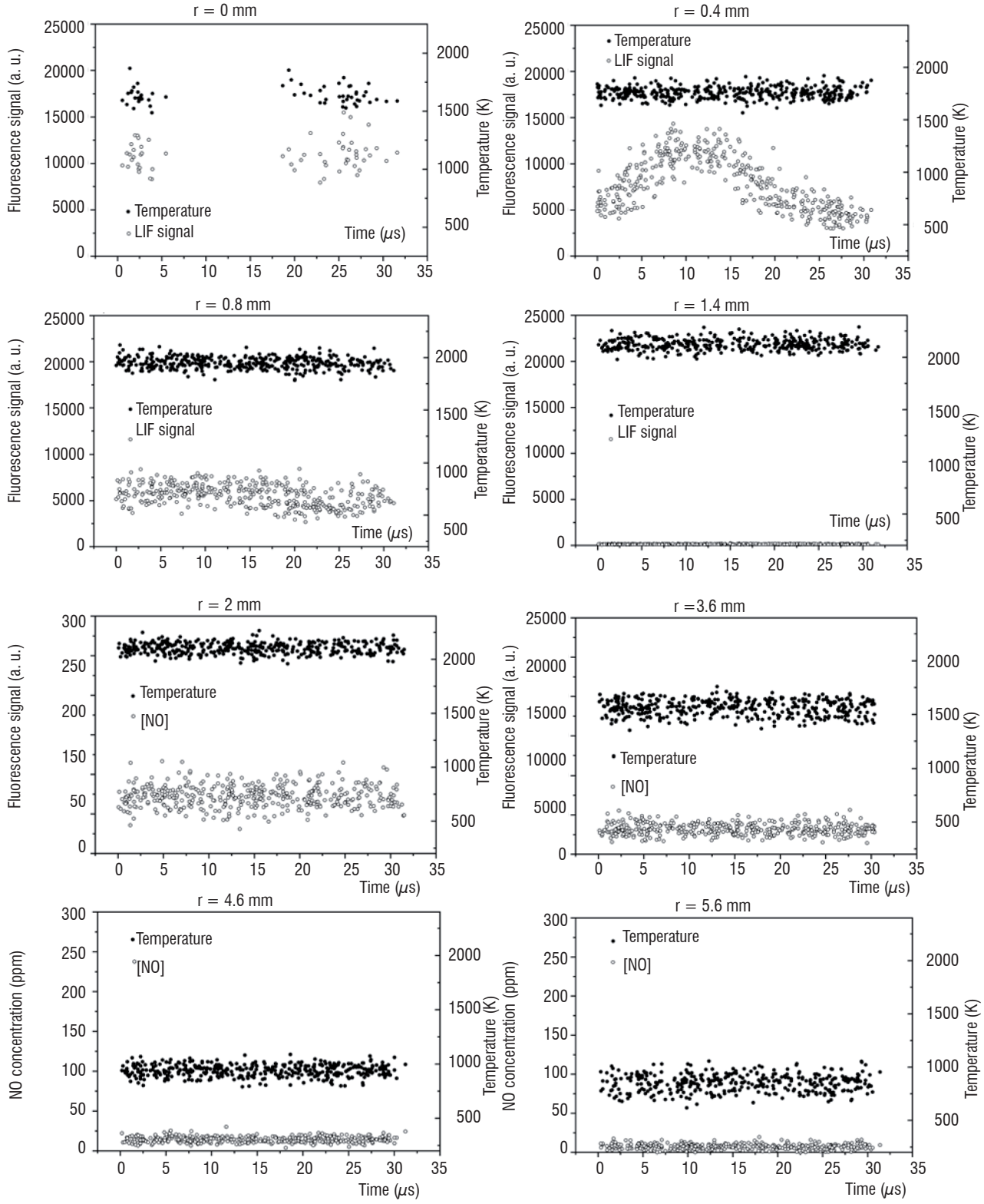

Figure 13 - Temporal evolution of the temperature and NO concentration inside the monodispersed droplet stream.

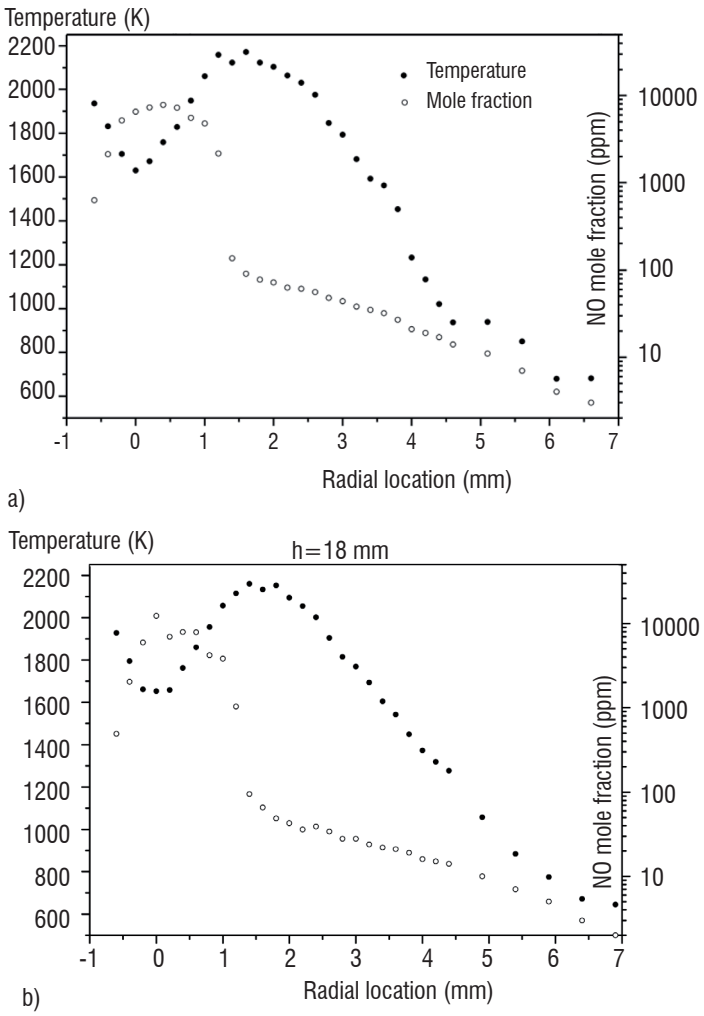

Figure 14 - Averaged profiles of temperature and NO mole fraction in the droplet stream injected at (a): 33200 Hz and (b): 16700 Hz.

The concentration of the parasite species is maximum on the droplet axis. Therefore, it seems to indicate that the signal originates from a reaction product appearing near the flame front, in the cooler region. Although the exact nature of the ethanol derivative is not known, it is probably C2H5O isomers resulting from decomposition of the fuel. Finally, the temporal evolution of these products can be compared to the change in vapour concentration which occurs near the droplet surface. In effect, the dynamic of the evaporation is influenced by the experimental burning rate between r=1 and 5 droplet diameters [13]. The radicals, which are produced through a transient process over the droplet period, reach a maximum concentration at r=5 dia. for C=6 and r=4dia. for C=3. The efficiency of that production is assumed to result from the aerodynamic drag effect.

Nanosecond discharge in CH_4/air flow

The time and spatial resolution of these techniques is now illustrated in the study of plasma-assisted combustion. Experimental investigation of a non-equilibrium nanosecond pulsed discharge at atmospheric pressure has been carried out [14]. The plasma is produced by a repetitive pulse generator and electric pulses of 10-40 kV in amplitude and 70 ns in duration with a pulse repetition frequency up to 200 Hz are produced. The high-voltage pulse generator is built using a hydrogen thyratron. Thanks to that system, triggering synchronization

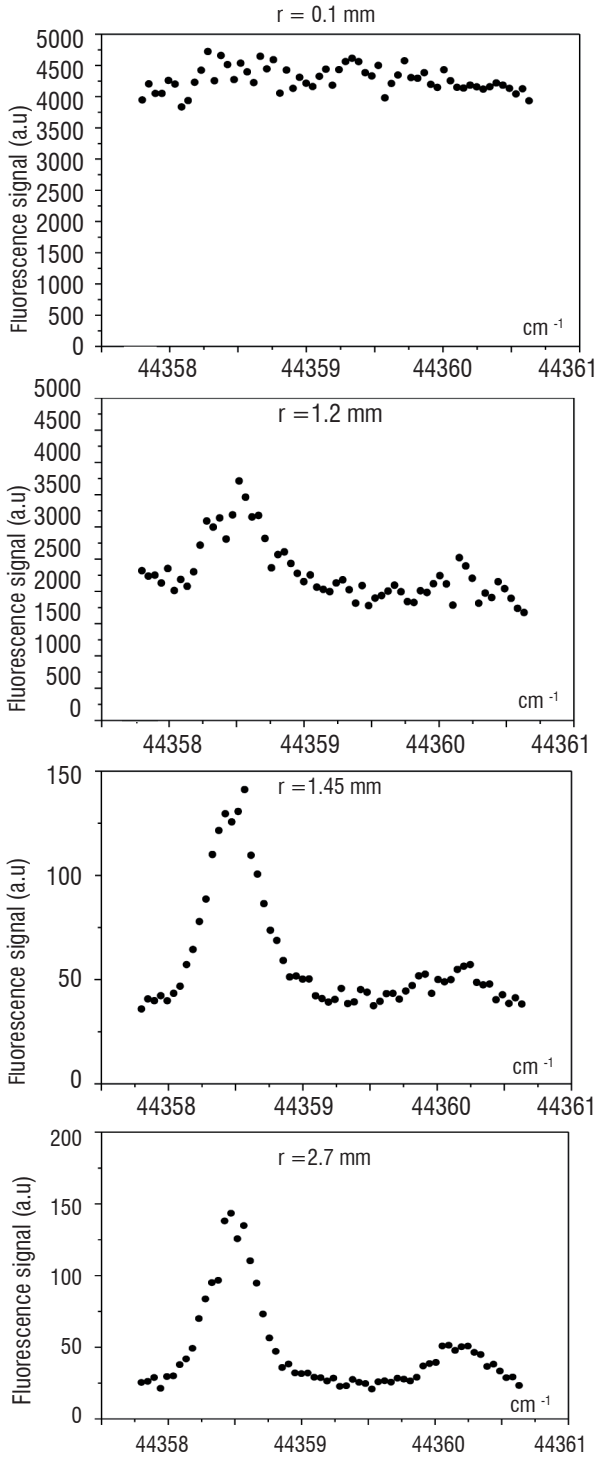

Figure 15 - Spectral evolution of the NO LIF signal versus radial location in the droplet stream in combustion.

is possible with a small jitter by using a pulse/delay generator. A jitter of about 10 ns is achieved, allowing good synchronization of the lasers with the pulsed discharge. Two stainless-steel needles, with a curvature radius at the tip of 0.1 mm are placed above the nozzle exit to produce the discharge (Figure 8). Positions of the needles with respect to the nozzle could be varied horizontally and vertically. Both electrodes are tilted vertically by 9° with respect to the propagation of the laser beams in the discharge. In this way, the laser beams can be focused at the centre of the discharge (Figure16).

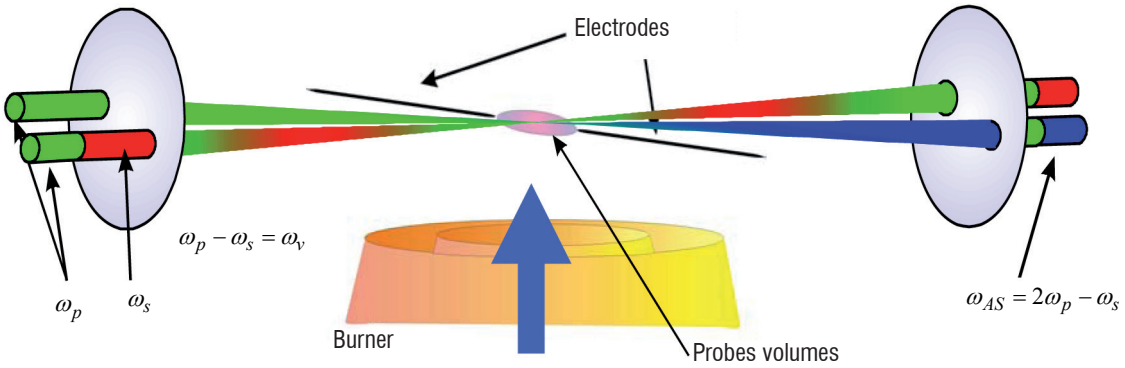

Figure 16 - Geometry of the excitation above the nozzle and between the electrodes.

Time-resolved CARS measurements are reported in the discharge. Experiment is performed in pure air and in mixture of methane and air. Spatial and temporal evolution of temperature and species distributions are recorded by delaying the probe lasers relative to the discharge pulse in the range 10 ns^{-1} ms.

The gases are flown from two concentric nozzles made of ceramics which is an electrically non-conductive material used to avoid electrical disturbances of the discharge. The inner injection nozzle is 10 mm diameter and is surrounded by an annular nozzle which is 20 mm in diameter. The inner nozzle operates with a methane/air mixture, while inert gas is injected through the surrounding nozzle to prevent chemical and hydrodynamical disturbances of the inner flow. Temperature measurements are performed using N_2 CARS thermometry. These measurements are intended to quantify the energy transfer in the gas mixture. It is demonstrated that energy transfer induced by collisions of N_2 with CH_4 considerably increases the thermal heating of neutral molecules at temperatures up to 2500 K (Figure 17). Effect of the discharge on the local temperature also allows to ignite the CH_4/air mixture for equivalence ratio ranging from 0.7 to 1.3 [15]. Fast development of a flame kernel was observed. The experiment also shows that the flame can be sustained above the discharge due the repetitive ignition of the flame at the plasma repetition rate. Then, the CARS investigation of major species such as CH_4, H_2 and C_2H_2 is performed as a function of time, (Figure 3). The evolution of the species is monitored over more than 1ms. The results are shown in figure 18 [15]. The CH_4 consumption and H_2 and C_2H_2 formation are localized and further calculations are under progress to identify that particular chemistry.

The experiments have demonstrated that a strong vibrational non-equilibrium can be sustained in N_2 at 1 bar. The effect of different colliding partners on the vibrational relaxation of N_2 is studied in CH_4/air mixtures with different equivalence ratio. The observed temperature distributions suggest that thermal equilibrium is not fully achieved.

Finally, the characterization of electron temperature and density was successfully performed using laser Thomson scattering (LTS) in the plasma (see Box 1).

Laser induced Gratings

Laser induced gratings consist in “printing” grating (index or coherence) into the flowing gas molecules. The time evolution of this printed gratings, determined by laser diffraction, gives access to a wealth of gas parameters such as speed or temperature.

Thermal

Laser-induced thermal gratings (LITG) have been described theoretically and we recall the derivation procedure of the main expressions driving the LIG signal temporal shape when the pump frequency is resonant with a one-photon transition of the probed molecules. The process is also described as the inelastic scattering of the wave “ ω_2 ” by the laser grating induced by the two waves at “ ω_1 ” (Figure 19).

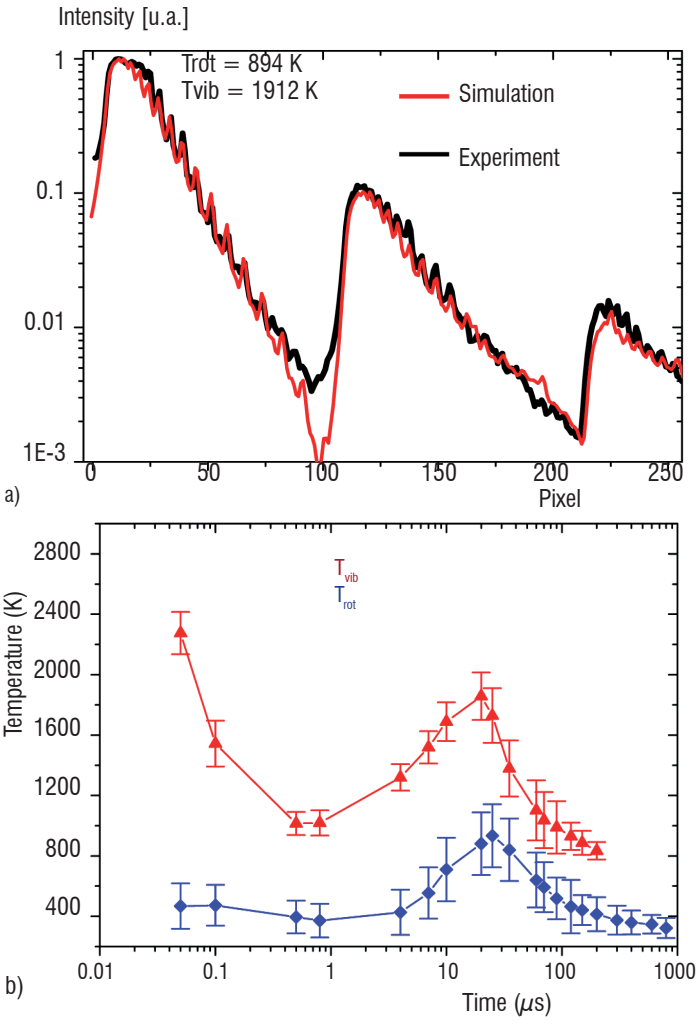

Figure 17 -(a): N_2 CARS spectra at a delay of 60 μs relative to the pulse discharge, spectral resolution of the multiplex CARS experiment is 0,25 cm^{-1}; (b): temporal evolution of the vibrational and rotational temperatures

Box 1 - Thomson Scattering

Laser Thomson scattering (LTS) is a powerful method for studying electron properties (electron density and temperature) in glow discharge plasmas occurring in gases having electron density in the range of 10^{15}-10^{20} m^{-3} [16]. LTS is the scattering of laser radiation by free electrons, when photon energy is small compared with the energy equivalent to the rest mass of the charged particles. The energy lost by the radiation is accounted for by the classical theory as a result of the radiation emitted by the charged particles when they are accelerated in the transverse electric field of the radiation. Because the electron mass is several orders of magnitude less than that of ions, the acceleration of electrons is larger for a fixed electric field. Therefore, we usually observe LTS only from electrons. The principle and general experimental arrangement of LTS is briefly presented. The Thomson scattering intensity $I_T(\Delta\lambda,\theta)$ is deduced from, $I_T(\delta\lambda,\theta)\,\Delta\Omega\,\delta\lambda = I_0 ne\,\Delta V\,d\sigma_T(\delta\lambda,\theta)\,\Delta\Omega\,\delta\lambda$ (A)
In this expression, the differential Thomson scattering cross section $d\sigma_T(\Delta\lambda,\theta)$ is given by :

$$d\sigma_T(\delta\lambda,\theta) = r_0^2(1-\sin^2\theta\cos^2\xi)\,S(\delta\lambda,\theta) \quad \text{(B)}$$

The scattering parameter α is defined by:
$\alpha = 4\pi/\lambda i \sin(\theta/2)$
When the scattering parameter α is $<< 1$, the radiation is incoherently scattered as in spontaneous Raman scattering. It consists in a simple summation of contributions from individual electrons. For the present experimental condition, the scattering is in this incoherent domain, e.g., $\alpha = 0.02$ from typical values of electron density (N_e=1 x 10^{18} m^{-3}) and electron temperature $(T_e = 3\ eV)$ with laser wavelength of 532 nm and a scattering angle of 90°. The electron velocity distribution $S(\Delta\lambda,\theta)$ is assumed to be Maxwellian. Electron temperature is measured from its half width at half maximum (HWHM). The electron density ne is obtained from Eq. A. By calibrating the detection system, the scattered light intensity measured by integrating over the spectrum gives the absolute electron density. Absolute calibration is performed in our case by using the spontaneous Raman scattering from N_2, with a known Raman cross section.

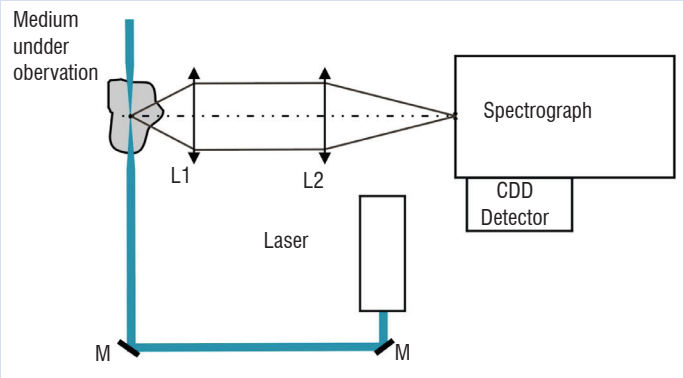

Figure B1 - 01 - Schematic diagram of the laser Thomson scattering apparatus

The experimental setup is presented in Figure B1 - 01 [17]. The laser beam at 532 nm (Nd: YAG) delivers 10 mJ per pulse at a repetition rate of 10 Hz. It is focused within the pulsed discharge using a 500 mm focal length lens. The Thomson scattered light is collected by an 80 mm focal length lens and imaged onto the spectrograph entrance slit using a 200 mm focal length lens. The Raman spectrograph (Jobin-Yvon T 64000) was especially designed to provide a good noise rejection. It has a 640 mm focal length and an f-number of 7.5. Its three 1800 grooves.mm^{-1} diffraction gratings allow good rejection of the light emitted at the excitation wavelength (Rayleigh, Mie and stray light). The spectrum is detected on a back-thinned liquid nitrogen cooled CCD-camera (800 × 2000 chip, Jobin-Yvon), providing quantum efficiency of 85 % at 500 nm. The dark current is lower than 3 e^-/pixel/hour and the readout noise is about 3 - 4 counts. The spectral resolution of the system is given by the spectrograph (0.003 nm/pixel). The whole optical system is mounted on a high precision three-axis remotely-controlled translation stages, allowing the displacement of the probe volume across the plasma.

The LTS setup is aligned and calibrated by recording the rotational Raman spectrum of air. The LTS spectrum is recorded over a spectral window of 200 cm^{-1} located at about 30 cm^{-1} from the excitation wavelength. The spectrum is integrated over a period of 1 min to improve the signal-to-noise ratio. In this case, the peak intensity of the Thomson signal is typically equal to 500 photoelectrons. No interference from the Rayleigh or from stray light has been observed, demonstrating the high noise rejection of the spectrograph. The procedure consists in recording the plasma emission without any laser beam before to record the LTS spectrum. The LTS light together with the plasma emission is then recorded after sending the laser beam in the plasma. The net Thomson scattering spectrum is obtained by subtracting the plasma emission from the raw Thomson spectrum. The absolute intensity is obtained from the Raman spectrum recorded before every measurement. The Thomson spectrum is then fitted using a Gaussian profile (electron velocity distribution function). The fit is obtained using a least-squared method. In the fitting procedure, only the wings of the profile are used. The electron density and the electron temperature are drawn from the fit.

In Figure B1 - 02, Thomson measurements are performed at different delays from the high-voltage pulse providing the temporal evolution of electron temperature and electron density during the discharge pulse. Measurements at $\Delta T = 20$ ns, show that electron temperature is about 2.6 eV and electron density is 10^{15} cm^{-3}. These values obtained at P = 1 bar and T = 300 K, allows to calculate the physical parameters characterizing the plasma; A Debye length of 3.7 10^{-7} m, a mean gap between electron of 10^{-7} m, a Landau radius of 5.7 10^{-10} m and an electron mean free path of 9.6 10^{-4} m. The ionization factor estimated to be 4 10^{-5} allows to conclude that this plasma is weakly ionized.

Measurements performed at larger delays (between 30 and 70 ns) show a fast decrease of electron temperature (from 2.6 to 1 eV) and a reduction of electron density by a factor of 10. This last value is in accordance with the reduction of electrical current by a factor of 8, demonstrating then the potential of LTS to measure the electron properties of these nanosecond pulsed discharges.

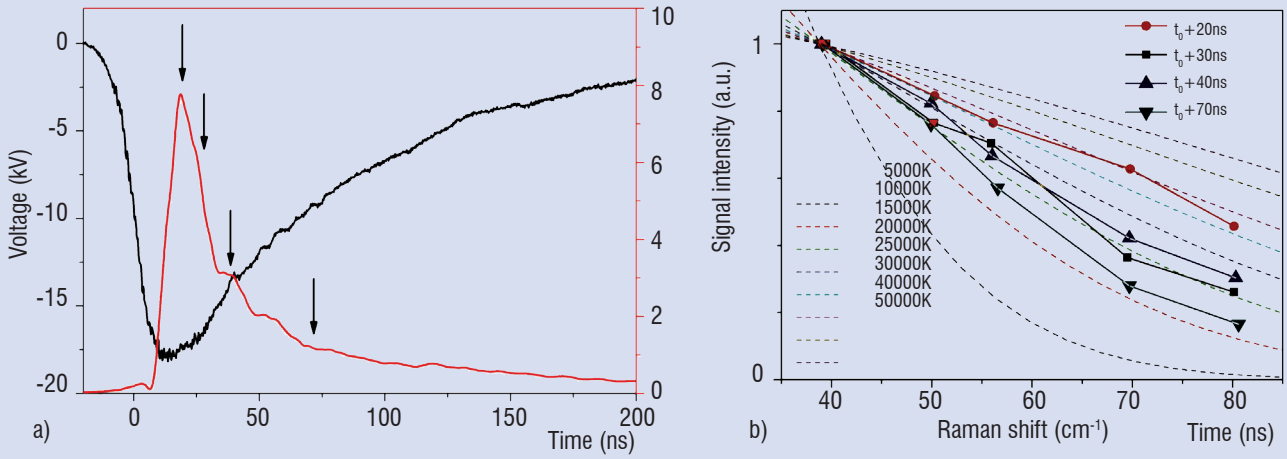

Figure B1 - 02 - (a): temporal delays relative to the discharge trig at which LTS measurements are performed; (b): experimental-theory comparison of LTS signals versus Raman shift with indication of electron temperatures.

Model description

The temporally overlapping crossed pump beams with parallel polarizations interfere and form an intensity grating. The fringe spacing Λ of the interference pattern is given by Bragg's law [18]:

$$\Lambda = \frac{\lambda_p}{2 \sin\theta} \qquad (3)$$

where λ_p is the wavelength of the pump beams and 2θ is their crossing angle. Pump beams energy resonantly absorbed by the molecules may be collisionally redistributed in the course of different non-radiative de-excitation processes, also referred to as quenching processes. They may take place even on the time scale of the coherent interaction characterizing standard four-wave mixing and represented in Figure 1. Collisional relaxation of spatially-periodic excitation may generate respective variations of temperature and density in the gas medium, which produce modulations of the complex refractive index; the phenomena is referred to as laser-induced gratings. The LIG signals are formed when the probe laser beam is diffracted by this regular modulation in the Bragg phase-matched direction, at the angle θ_B to the optical axis. The temporal evolution of the diffraction efficiency η is mainly determined by the time scale of the relaxation processes and can be recorded by using cw or long-pulse probe radiation, or by varying the delay between the probe laser pulse with respect to the pump laser one. The latter technique was used at Onera to probe NO_2 [19, 20].

Probing of mixtures

We present an application of the LITG technique to the detection of NO_2 molecules seeded in an atmospheric pressure flow [19] and flame [20]. The beams were focused in the geometry of figure 19. The temporally delayed short pulses of pump and probe radiation were used in the experiment.

The pump and probe beams have horizontal polarization. They are made collinear by means of a dichroïc mirror (D1). The three beams are aligned in a planar forward BOXCARS geometry (Figure 2a) and focused using an achromatic lens (L1) with a 500 mm focal length. The energy of each of the pump beams in the probe volume is typically about 1.5 mJ. In this case, a power density of about 1.6 GW/cm^2 is obtained at the focus with a beam diameter of about 100 μm. The crossing angle of about 1.9° provides a fringe spacing of $\Lambda = 12 \pm 0.5$ mm. A dichroïc mirror (D2) is installed into the path of the pump beam (1) in front of the focusing lens in order to suppress the stray light from the probe beam in the direction of the signal beam. It was found that filtering at this location is particularly efficient to suppress scattering by the nearby optics inserted into the probe beam (3), that is separated by only 22 mm from the pump beam (1). The recollimated LITG signal beam is filtered out by means of pinholes inserted into the detection path which is about 12 m long. A set of 6 mm OG570 (Schott glass) colored filters (CF) is positioned after the first pinhole to reduce the scattered light of the pump laser. The signal is registered by a photomultiplier tube (XP1017, Philips).

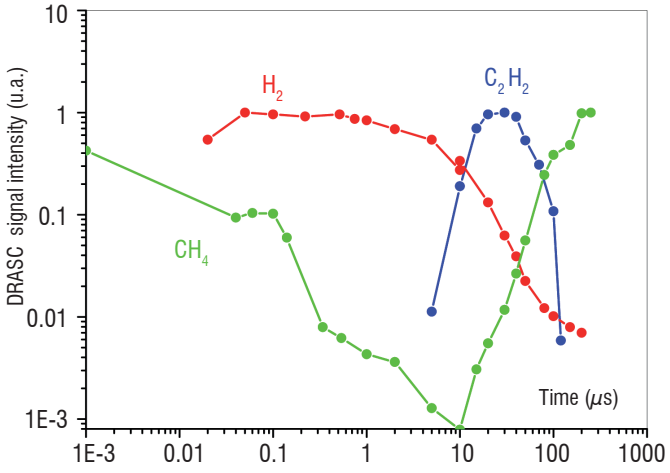

Figure 18 - Temporal evolution of H_2, CH_4 and C_2H_2 sampled by CARS over 1 ms after the discharge pulse.

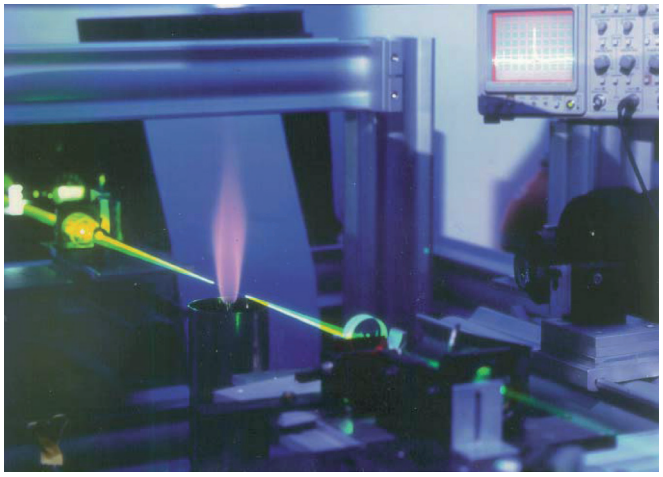

Figure 20 - View of the seeded flame and of the pump (green) and probe (yellow) lasers used for LITG experiment.

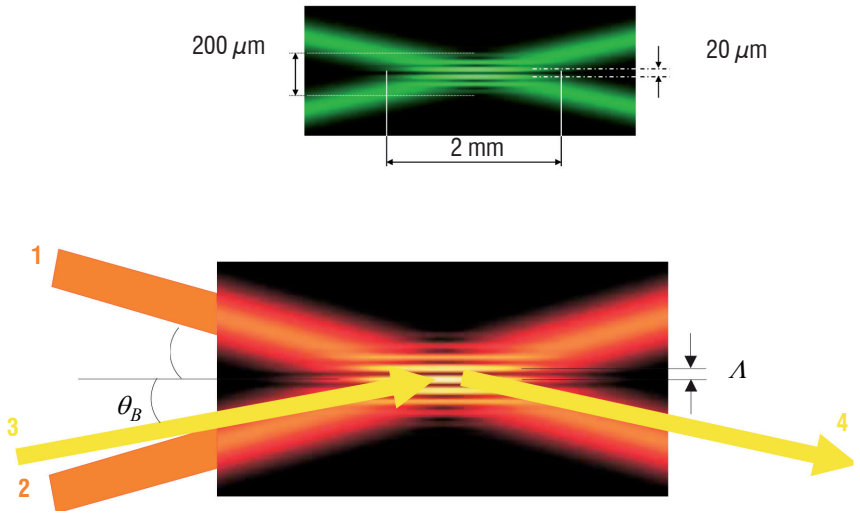

Figure 19 - Principle of the LITG excitation; the two strong pump beams (1) and (2) induce the grating on which the probe (3) is diffracted.

The signals from the detection channels are gated, integrated using an electronic unit (E) and processed by a computer (PC), using the acquisition routine. An average of 10 to 100 laser shots can be taken in each measurement condition.

The burner is presented in Figure 20. It is a coaxial jet assembly composed of a short tapered-contour fuel jet nozzle, of 10 mm inner diameter, located at the axis of an annular cylindrical cavity for air flow, with 80 mm external diameter. This cavity is filled inside with small glass balls providing conditions of laminar air flow around the central jet. The fuel is a mixture of hydrogen (or methane) with nitrogen.

To analyze the characteristics of the LITG signals, the transversal temperature profiles of these two flames should be known. We used N_2-CARS to perform these measurements at a height h = 2 mm above the plane of the nozzle orifice. The spatial resolution of CARS measurements employing a lens with a focal length of 300 mm was 3 mm. For CH_4/air flame the flowing gases in the burner were the following: 1.44 l/min of CH_4 and 0.55 l/min of N_2 seeded with 0.1 % of NO_2, that provided NO_2 concentration of 276 ppm, were being supplied to the nozzle, while 71.0 l/min of air were being delivered to the peripheral annular cavity. The radial temperature profile of this flame is shown in Figure 21(a). For H_2/air flame 5.9 l/min of H_2, 1.48 l/min of pure N_2 and 0.35 l/min of N_2 seeded with 1 % of NO_2, corresponding to NO_2 concentration of 453 ppm, were being supplied to the nozzle, while 60.3 l/min of air were flowing at the periphery. The corresponding radial temperature profile is shown in Figure 21(b). The reaction zone is slightly closer to the burner axis for CH_4 (r = 7.5 mm) than for H_2 (r = 8.0 mm). Temperature profile has a marked influence on the radial variation of the LITG signal in these two flames.

Temporal evolution of LITG signals was recorded by varying the delay between the pump and probe pulses to determine the dependence of the signal strength on NO_2 concentration, on type of a buffer gas (or fuel), and on temperature at various positions inside the flame. Thermal grating signals are generated through the thermalization of energy resonantly absorbed by NO_2 molecules. We have investigated the dependence of LITG signals on temperature and gas composition in figure 22 and 23. Theoretical description of the signal strength and temporal evolution was performed following the approach employed in [18-20]. Comparison of experimental results with theoretical predictions is shown. LITG signal in a cold CH_4 flow at 1 bar and 300 K is presented in Figure 22(a). The flow supply was the following: 1.67 l/min of CH_4 and 0.7 l/min of N_2 seeded with 0.1% of NO_2 (295 ppm of NO_2) - through the nozzle, and 12.5 l/min of air - through the annular cavity. In the CH_4/air flame, LITG signal was detected at two radial positions: r = 0 mm (Figure 22b) and r = 3.1 mm (Figure 22c). LITG signal in a cold H2 flow at 1 bar and 300 K is shown in Figure 23(a). The flow supply was 3.0 l/min of H_2 and 1.1 l/min of N_2 seeded with 0.1% of NO_2 (250 ppm of NO_2) -

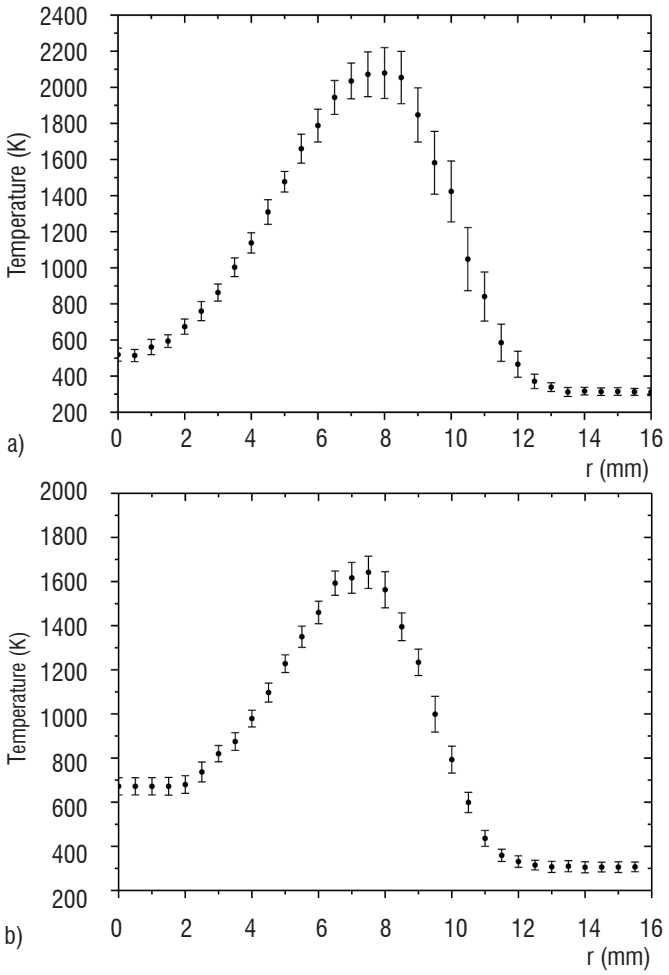

Figure 21 - CARS profiles of temperature measured on N_2 molecules in the two flames; (a): H_2/air and (b): CH_4/air.

through the nozzle, and 10 l/min of air - to the periphery. In the H_2/air flame, signal was detected at r = 0 mm (Figure 23b) and r = 2 mm (Figure 23c).A comparison of Figures 22 and 23 shows that in H_2 the lifetime of the thermal grating is relatively small, and hence the signal amplitude is damped over a shorter time scale, as opposed to CH_4. The dip between the two oscillation peaks is still visible at 300 K (Figure 22a), and vanishes at higher temperatures (Figures 22 b,c). The disappearance of the resolved oscillation peaks leads to lower accuracy in the non-linear fitting of signal shape that may provide less defined information in case of H_2 as compared to CH_4.

Finally, the sensitivity of the technique to NO_2 detection was measured under the flame conditions (Figure 24) and the estimated detectivities are given in tables I and II. It is seen that non linear techniques offer a quite good sensitivity level as compared to absorption on NO_2 [29] and offer an unique possibility to produce stronger signal when pressure increases.

Coherent and Electrostrictif

Here, we demonstrate that coherent Raman scattering is able to provide the velocity from the Doppler shift in low-pressure high speed flows while a more collective process like Brillouin scattering can be applied to measure the velocity in higher pressure conditions. These two techniques can be implemented either separately or in combination to measure simultaneously temperature, density and velocity over a large domain of flow fields. As shown below, the proposed approaches are based on the analysis of the time evolution of dynamic gratings (coherent or electrostrictif gratings [21]) produced by crossing two coherent pump beams, see Figure 19.

Time-domain coherent anti-Stokes Raman scattering

The CARS velocimetry technique is based on a single-shot time sequence where the anti-Stokes signal generation results from the application of a long pump (20 ns) and a short Stokes (1 ns) pulses, in the folded boxcars geometry. These two pulses are synchronised such that the Raman excitation which is coherently driven during the Stokes pulse application, is continuously probed by the long pump pulse (Figure 25). If the signal is produced in a low-pressure supersonic jet, the Raman coherence keeps oscillating freely after the Stokes interruption; during this free decay, the anti-Stokes shows a damped oscillation, which frequency gives the jet velocity. The anti-Stokes free decay oscillation can be readily explained by use of a grating picture. As previously introduced, crossing the two pump beams in the boxcars geometry leads to a periodic spatial modulation of the light intensity (Figure 19). This grating being illuminated by the short Stokes pulse, a spatially-modulated Raman excitation is printed within the gas leading to a coherence grating that is matched with the pump grating. When excitation stops, the coherence grating moves with the jet velocity; thus, the coherence and pump gratings are successively in an out of phase leading to a temporal modulation of the anti-Stokes response from which the velocity can be deduced. Furthermore, the translational temperature can be obtained from the time decay of the anti-Stokes signal which is imposed by the thermal motion of the molecules in the Doppler regime [22].
The performances of the Raman approach have been tested in a low-enthalpy Mach 10 wind tunnel delivering a uniform laminar flow in 90 s-long runs. The flow conditions are Vjet = 1382 ms^{-1}, static temperature = 48 K and static pressure = 5.5 Pa. The main objective of the experiment was the characterization of the thermodynamic behaviour of a laminar flow through a bow shock generated in front of a cylinder (16 mm diameter, 100 mm long). The axes of the CARS probe volume (14 mm long and 0.2 mm diameter) and the cylinder are aligned parallel to each others so that the velocity profile is recorded along the stagnation line (Figure 26). The optical CARS bench comprised two main parts:

- an injection-seeded Nd: YAG laser delivering 20 ns, 40 mJ pump beams at 532 nm
- a parametric source composed of a doubly resonant optical parametric oscillator followed by an optical parametric amplifier to deliver the 1.5 ns Stokes pulse around 535 nm [29].

The Stokes wavelength is adjusted to probe pure rotational Raman lines (S-branch) of nitrogen so as to take advantage of a long decay time of the Raman coherence [23]. Velocity measurements obtained by time domain CARS are reported in Figure 26. In addition, rotational temperature and density measurements obtained from dual-line CARS [24] are also reported in this figure. The different experimental profiles demonstrate the strong variations of the thermodynamic parameters through the shock:

- rotational temperature jumps from its static value (48 K) to the stagnation temperature (1058 K) as a result of the energy re-distribution between the different degrees of motion through the shock;
- gas density increases by a factor 6 as expected from a Navier-Stokes calculation;
- velocity variation is higher than 1 km s^{-1} within 0.3 mm through the shock, i.e. in the time duration of one or two collisions. These experiments illustrate the ability of CARS to capture strong velocity, temperature and density gradients.

In the collisional regime (several tens of hPa), the decay time of the Raman coherence is reduced to a few tens of picoseconds, precluding the potential use of time-domain CARS for velocity measurements. Hence, at high pressure, methods based on the time analysis of long persistent gratings such as thermal or electrostrictive gratings become more appropriate to get the flow velocity. As previously proposed [25], an elegant approach to get simultaneously temperature, velocity and density relies on the combination of two coherent techniques i.e. Raman and Brillouin scattering implemented with common pump lasers in the classical BOXCARS geometry (Figure 2a). Basically, temperature and density measurements are obtained from classical broadband CARS while the velocity is deduced from the temporal analysis of the two acoustic waves that are generated in opposite directions through electrostritive effect induced by the two crossing pump beams, see Figure 27 a).The experimental setup is depicted in Figure 27 b). A pulsed, injection seeded Nd: YAG laser, operating at 10 Hz, provides two excitation pump beams at 532 nm. The pulse duration is 15 ns (FWHM), the beam diameter is 4 mm and the total energy is 45 mJ per pulse. The excitation beams are focused by means of a 240 mm-focal length achromatic lens, with an angle of 2.9° ±0.1°. This results in a probe cylinder of approximately 2 mm in length and 30 μm in diameter; the corresponding grating wavelength is 10.56 μm. The read-out laser is a continuous wave argon ion laser, which delivers 400 mW in single-line operation at 458 nm. The probe beam intersects the grating at the Bragg angle θ_B. Figure 27 b) also shows the Stokes beam produced at a 607 nm central wavelength by a dye laser (energy per pulse = 2 mJ) for probing the Q-branch of nitrogen. After spectral separation of the Brillouin and CARS signals using a spectrometer, the time evolution of the Brillouin signal is recorded using a fast photomultiplier (Hamamatsu R2566U) while the CARS spectrum is dispersed on a CCD detector (Princeton ICCD - 512T).

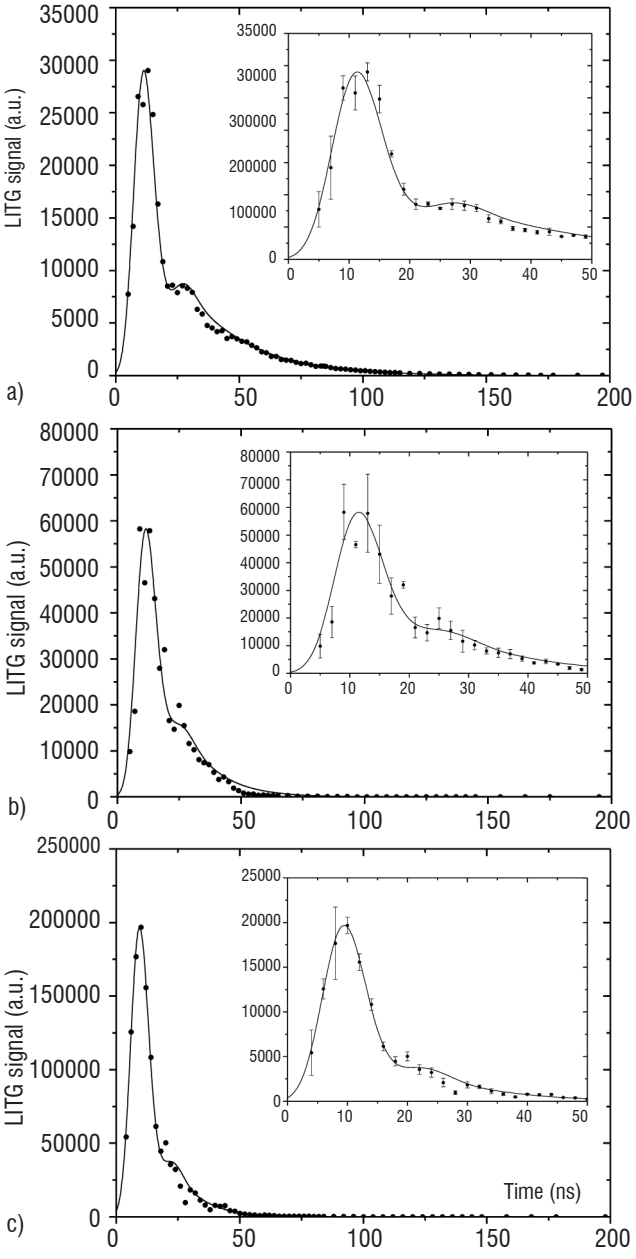

Figure 22 - LITG signal evolution measured (a) in the cold H_2/air mixture and in the H_2/air flame at two radial positions, (b): r = 0 mm and (c): r = 2 mm.

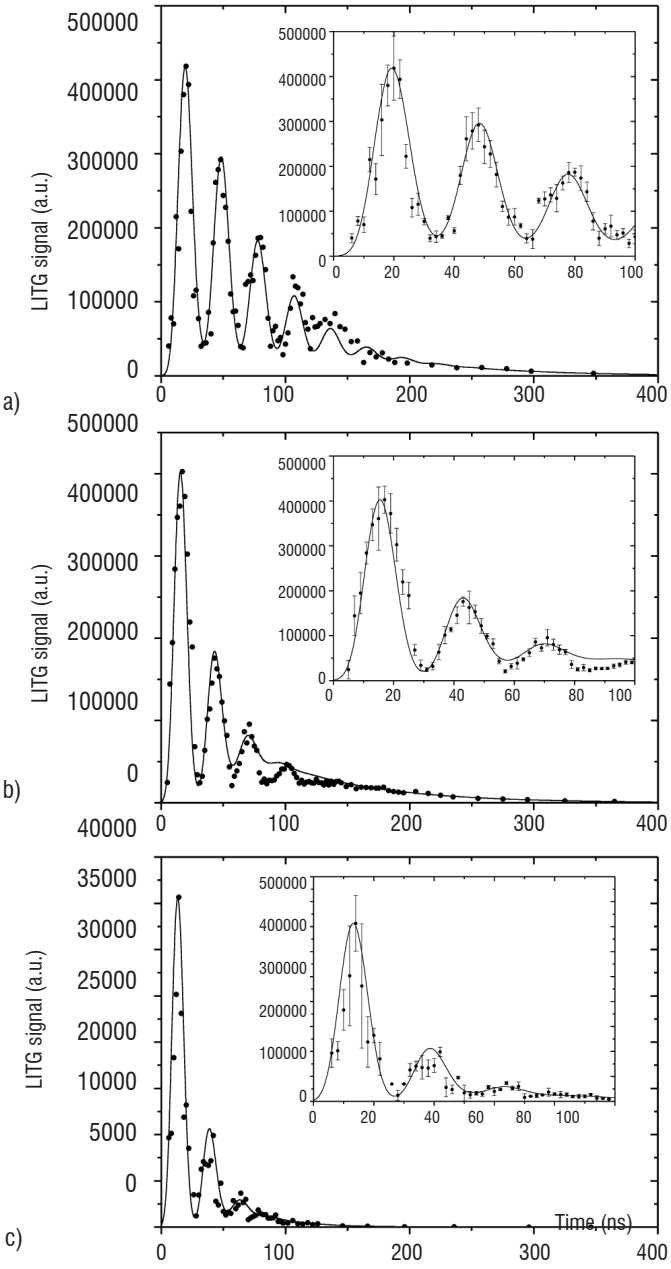

Figure 23 - LITG signal evolution measured (a) in the cold CH_4/air mixture and in the CH_4/air flame at two radial positions, (b): at r = 0 mm and (c) at r = 3.1 mm.

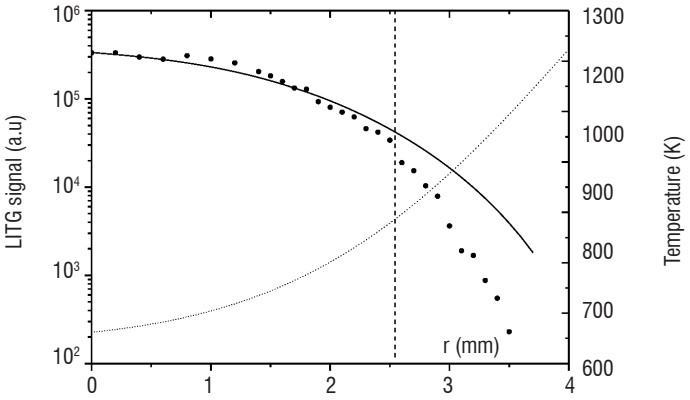

Figure 24 - NO_2 radial profile obtained by LITG in the CH_4 /air flame; the signal is decreasing toward the flame, located at r=8mm, because temperature is increasing and then because of NO_2 destruction beyond 3 m; measurements(••••), calculation (—) [18] and temperature (dotted). Dashed vertical line indicates the nozzle radius.

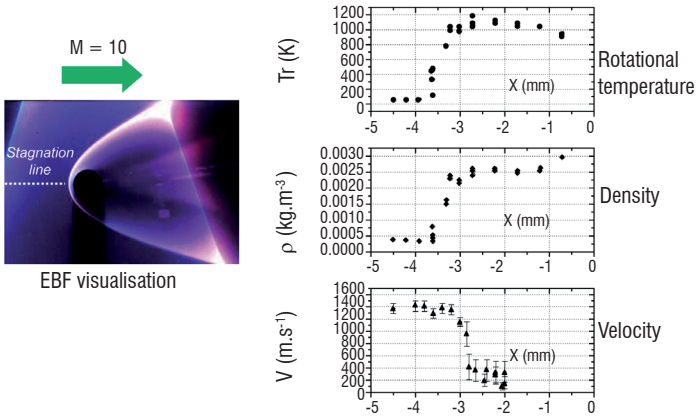

Figure 26 - CARS measurements through a bow shock ; Electron beam fluorescence (EBF) vizualisation of the shock (left) ; CARS measurements along the stagnation line (right).

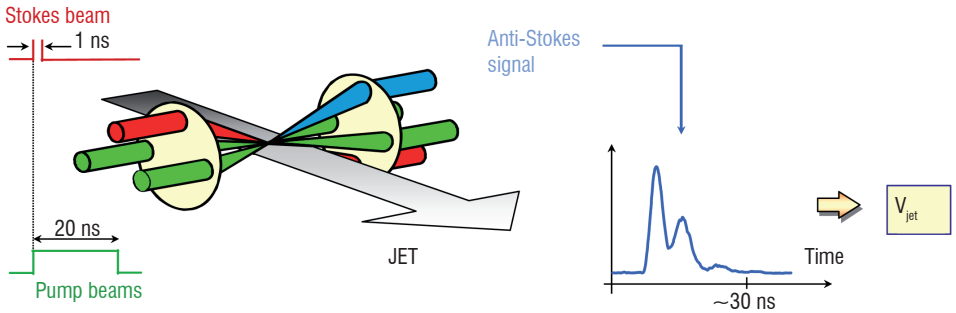

Figure 25 - Illustration of the time-domain CARS technique.

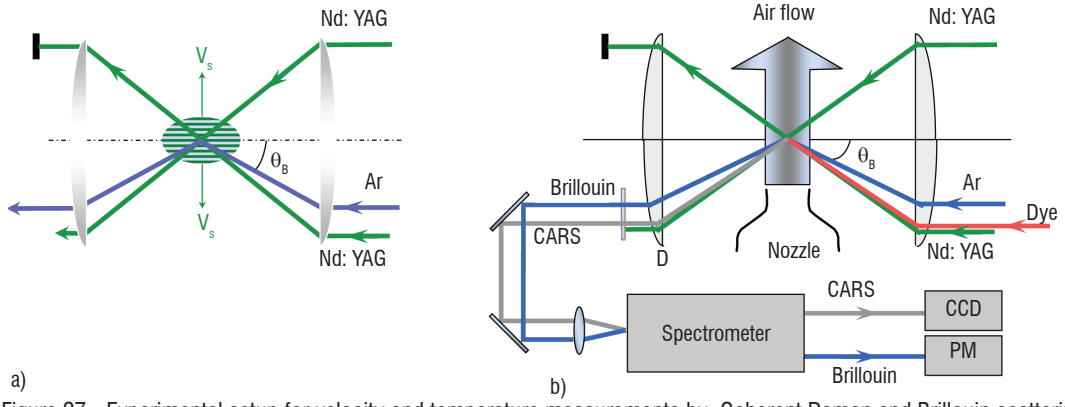

Figure 27 - Experimental setup for velocity and temperature measurements by Coherent Raman and Brillouin scattering.

The demonstration experiment has been carried out in a subsonic flow delivered by an étalon nozzle (Disa type 55D45, section = 60 mm^2). Two different beam configurations have been tested. In the first configuration, the argon spot beam was well superimposed with the pump grating whereas it was focused at a small distance ($\Delta x \approx 10\ \mu m$) apart from the pump gratings. The time-dependence of the Brillouin signals are reported in Figure 28 for both cases.

For well overlapping beams (Figure 28 a) in standing conditions (no flow), one obtains a damped oscillation which results from the interference of the two acoustic waves propagating in opposite directions within the probe volume. In presence of a 200 ms^{-1} flow velocity, the temporal dependence of the Brillouin signal changes significantly, one observes an oscillation with a tail which results from the different resident times of the two acoustic waves within the probe volume. For separated excitation and probe spots (Figure 28 b), the oscillating component disappears, and the signal is constituted of a hump. Only one sound wave meets the probe spot, after a time of flight $\Delta t1$. Figure 29 presents the results of simultaneous measurements of the CARS temperature (dots) and Brillouin velocity for the two beam configurations. These results are in good agreement with the expected values given by the Saint Venant formula, demonstrating the capability of the proposed approach.

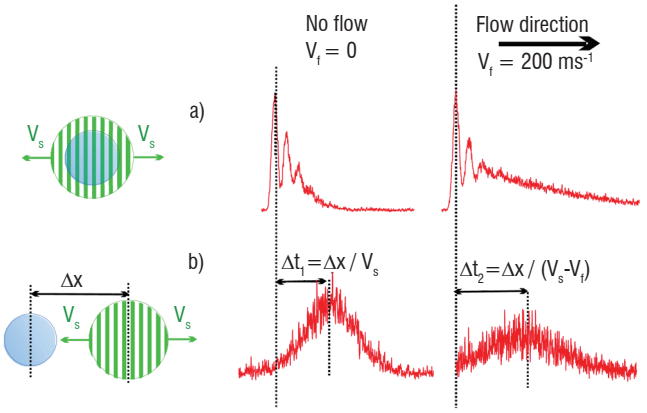

Figure 28 - Comparison of Brillouin signals obtained in a standing gas and a 200 ms^{-1} jet for two different beam configurations.

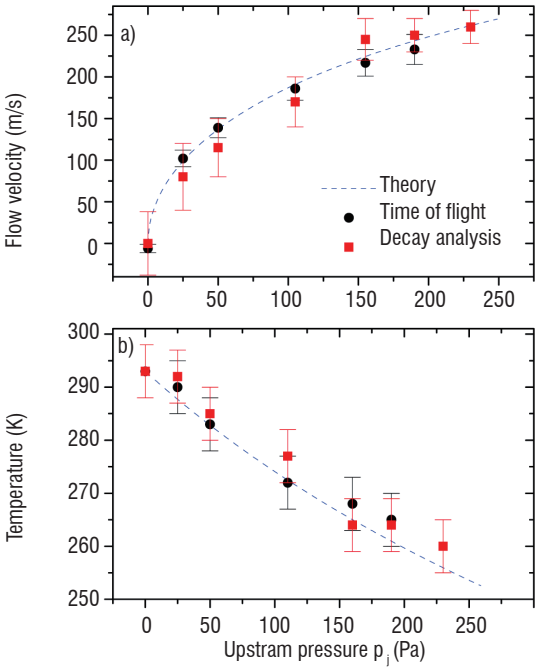

Figure 29 : Simultaneous velocity and temperature measurements obtained for different upstream pressures; experimental data have been obtained for the two beam configurations shown in Fig.28: 'decay analysis' is for the a) configuration while 'time of flight' is related to the b) configuration.

Conclusion

The experiments presented in the present paper have demonstrated the potential of non linear techniques and the interest in combining different techniques in situ. The choice of the techniques is relevant to the media under study namely, highly luminous, or high temperature (pressure) or strong non equilibrium. In effect, they are carefully handled not to perturb the evolution of the flow and to retrieve quantitative measurements.

In the buoyant flame it was shown that [NO] closely follows the temperature, with the peak in the former being located in the bulge region. The large [NO] in the compressed flame arises, in part, from the transport of the NO generated in other regions of the flame, which was not seen before. The contradictory behavior of temperature and [NO], which increase/decrease in the compressed/stretched flame location, respectively, was also quantified by time-resolved measurements. The techniques provide absolute concentrations of radicals and molecules during a vortex/flame interaction; they can be used to identify the important chemical pathways in diffusion flames. In the droplet study, we have probed a liquid/ gas media, less complex than realistic spray, by providing accurate data to improve the knowledge of droplet–flame interactions. To our knowledge, this is the first demonstration of time resolved measurements in a self sustained ethanol droplet stream flame. It was also shown that a pulsed plasma offer the possibility to improve combustion of a premixed CH4/ air flame. The transient plasma has consistently shown significant reductions in ignition delay and increased lean burn capability relative to conventional spark ignition. The demonstration of Thomson scattering to infer electron density in such a plasma was made possible thanks to a particular set up. Finally, CARS measurements were applied through a bow shock and temperature and velocity were obtained using a combination of CARS and Brillouin scattering. In all cases, the combination of pertinent laser diagnostics has proved their unique ability to identify the physical processes and diagnose the thermodynamic conditions without any disturbance of the media ■

References

[1] K. KOHSE-HÖINGHAUS AND J. B. JEFFRIES - *Applied Combustion Diagnostics.* Taylor and Francis, New York, 2002.

[2] S. DRUET, J.P. TARAN - *CARS Spectroscopy*. Prog.Quant. Electronics 7, 1 1981.

[3] P. D. MAKER AND R.W. TEHUNE, Phys. Rev, 137, A 801 (1965)

[4] T. A. WASSERMAN, P. H. VACCARO, B. R.JOHNSON - *Degenerate Four-Wave Mixing Spectroscopy as a Probe of Orientation and Alignment in Molecular systems.* J. Chem. Phys. 108 (1998) 7713-7738.

[5] H. BERVAS, B. ATTAL TRÉTOUT, L. LABRUNIE AND S. LE BOITEUX - Il nuovo cimento. vol 14D, n°10, pp1043-1050, 1992.

[6] H. BERVAS, S. LE BOITEUX, B. ATTAL-TRÉTOUT, J. P. TARAN - *OH Detection and spectroscopy by DFWM in Flames: Comparison with CARS*. J. Phys. B: At. Mol. Opt. Phys. 25 (1992) 949-969.

[7] S. WILLIAMS, R. N. ZARE, L. A. RAHN - *Reduction of Degenerate Four-Wave Mixing Spectra to Relative Populations 1.* Weak-field limit, J. Chem. Phys. 101 (1994) 1072-1092.

[8] V. KRÜGER, M. DUMONT, S. LE BOITEUX, Y. J. PICARD, F. CHAUSSARD, B. ATTAL-TRÉTOUT - *FDFWM spectra of NO in the Strong Field Limit Including Polarization, Line Coupling and Multipole Effects.* I. Theory, II. Experiments, Phys. Rev. A, 64, 012716-1 and 012717-1, 2001.

[9] B. ATTAL-TRÉTOUT, P. BERLEMONT, J.-P. TARAN - *Three-Colour CARS Spectroscopy of the OH Radical at Triple Resonance*. Mol. Phys. 70 (1990) 1-51.

[10] B. LAVOREL, H. TRAN, E. HERTZ, O. FAUCHER, P. JOUBERT, M. MOTZKUS, TIAGO BUCKUP, TOBIAS LANG, HRVOJE SKENDEROVI, GREGOR KNOPP, PAUL BEAUD, HANS M. FREY - F*emtosecond Raman time-resolved molecular spectroscopy.* Comptes Rendus Physique, Volume 5, Issue 2, March 2004, Pages 215-229.

[11] ZUMBUSCH, G.R. HOLTOM, X.S. XIE - *Three-Dimensional Imaging by Coherent anti-Stokes Raman Scattering*. Phys. Rev. Lett., Vol 82, N° 20, p 4142 1999.

[12] F. GRISCH, B. ATTAL-TRÉTOUT, A. BRESSON, P. BOUCHARDY, V. R. KATTA, W. M. ROQUEMORE - *Investigation of a Dynamic H2-Air Diffusion Flame With Advanced Optical Diagnostics And Numerical Modeling.* Combustion and Flame, 139,28-38 (2004).

[13] J.F. VIREPINTE, O. ADAM, G. LAVERGNE, Y. BISCOS - *Droplet spacing on drag measurement and burning rate for isothermal and reacting conditions. Journal of Propulsion and Power.* Vol. 15, pp 97-102, 1999.

[14] D. PACKAN, F GRISCH, AND B. ATTAL-TRÉTOUT - *Study of plasma enhanced combustion using optical diagnostics.* AIAA paper 2004-0983, 42nd AIAA AerospaceSciences Meeting and Exhibit (2004).

[15] D. MESSINA, B. ATTAL-TRÉTOUT, F. GRISCH - *Analysis of a Non-Equilibrium Pulsed Nanosecond Discharge at Atmospheric Pressure using Coherent anti-Stokes Raman Scattering.* Proceedings of the combustion institute, 31, pp 825-832 (2007).

[16] M. D. BOWDEN, Y. GOTO, H. YANAGA, P.J.A. HOWARTH, K. UCHINO, K. MURAOKA - Plasma Sources Science and technology 8 (1999), pp. 203-209.

[17] D. MESSINA, G.A. GRANDIN, B. ATTAL-TRÉTOUT, F. GRISCH. INCA meeting, Rouen (Coria), October 23-24, 2008.

[18] R. FANTONI, M. GIORGI, L. DE DOMINICIS, D. N. KOZLOV - *Collisional Relaxation and Internal Energy Redistribution in No_2 Investigated by Means of Laser-Induced Grating Technique.* Chem. Phys. Lett. 332 (2000) 375-380.

[19] E. LOUBIGNAC, B. ATTAL-TRÉTOUT, S. LE BOITEUX, D. KOZLOV - *Two-Color non-Linear Spectroscopy: Application to NO_2.* C.R. Acad. Sci. Paris, t. 2, série IV (2001) 1013-1027.

[20] E. LOUBIGNAC - *Etude du mélange à quatre ondes à deux couleurs dans les milieux en combustion : application aux composés azotés*. PhD thesis, Université de Bourgogne (2003).

[21] A. STAMPANONI-PANARIELLO, B. HEMMERLING, W. HUBSCHMID - *Temperature Measurements in Gases Using Laser-Induced Electrostrictive Gratings.* Appl. Phys. B 67 (1998) 125-130.

[22] M. LEFEBVRE, B. SCHERRER, P. BOUCHARDY, T. POT - *Transient Grating Iinduced by Single-Shot Time-Domain Coherent Anti-Stokes Raman Scattering : Application to Velocity Measurements in Supersonic flow.* J. Opt. Soc. Am., B13, n°3, 514 (1996).

[23] B. SCHERRER, A. GODARD, I. RIBET, P. BOUCHARDY, T. POT, M. LEFEBVRE - *Comparison of Dephasing Times for Vibrational and Rotational Coherent Anti-Stokes Raman Scattering : Implications for Velocimetry*. Appl. Phys., B71, 859 (2000).

[24] M. PÉALAT, M. LEFEBVRE - *Temperature Measurement by Single-Shot Dual-line CARS in Low-Pressure Flows.* Appl. Phys., B53, 23 (1991).

[25] M. RIBET - *Oscillateurs paramétriques optiques à cavités imbriquées pour l'étude des réseaux dynamiques créés par mélange à quatre ondes résolu en temps.* PhD Thesis Paris XI (2001).

[26] F. DUPOIRIEUX - *Optical Diagnostics Used at Onera to Characterize Turbulent ReactiveFlows and to Validate Aero- and Rocket Engine Combustor Modelling.* Aerospace Lab n°1, October 2009.

[27] F. GRISCH, M. ORAIN - *Role of Planar Laser-Induced Fluorescence in Combustion Research.* Aerospace Lab n°1, December 2009.

[28] G. LAVERGNE, Y. BISCOS, C. LAURENT, V. BODOC - *Advanced Measurement Techniques for Spray Investigations.* Aerospace Lab n°1, December 2009.

[29] A.K. MOHAMED, M. LEFEBVRE - *Laser Absorption Spectroscopy to Probe Chemically Reacting Flows.* Aerospace Lab n°1, December 2009.

Acronyms

SRS (Stimulated Raman gain Spectroscopy)
IRS (Inverse Raman Scattering)
CSRS (Coherent Stokes Raman Scattering)
RECARS (Resonance Enhanced)
LTS (Laser Thomson Scattering)
HWHM (Half Width at Half Maximum)
LITG (Laser-Induced Thermal Gratings)
CARS (Coherent Anti-Stokes Raman Scattering spectroscopy)

AUTHORS

Brigitte Attal-Trétout performed the first Coherent Anti-Stokes Raman Scattering spectroscopy (CARS) experiments at Onera. The so-called «resonant» version of CARS was created within this framework and used to record the first spectra of iodine. Since then, the Raman techniques and their degenerated version have been very widely applied to the measurement of low molecular concentrations. Brigitte Attal-Trétout has worked on the theme of optical metrology and non-linear spectroscopy applied to the diagnosis of reactive environments. She has directed a research unit and reoriented its work on diagnostics and plasmas. Brigitte Attal-Trétout is currently a director of research.

Frédéric Grisch, Masters degree in fluid mechanics in 1982, PhD in Energetics in 1988 and HDR in 2008 from the University of Rouen (France). Senior scientist at Onera/DMPH in charge of the development and application of laser diagnostics (CARS, PLIF, Raman scattering, Rayleigh scattering, Thomson scattering, etc.) for gaseous, liquid and solid propellant combustion, plasmas and nonreactive flow fields. Head of an Onera/CNRS research project on optical techniques for the investigation of multi-component spray evaporation.

Michel Lefebvre received his Ph.D. Degree from the University of Lille I and the Habilitation Degree in Optics from the University of Paris XI. He is currently senior scientist at Onera where he leads the 'Laser Sources and Sensing Physics' research unit in Palaiseau. He has conducted various studies in non linear optics and laser sources. He developed and applied the CARS technique to reactive flow and hypersonic wind tunnels. His current research covers parametric conversion processes and optical parametric laser sources.

Denis Packan received an Engineering Diploma from Ecole Centrale Paris (France) in 1996 and a PhD in Plasma Physics from Stanford University (USA) in 2002. He is currently a staff research scientist at Onera, Palaiseau, France where he is in charge of plasmas for aerospace applications, including space propulsion, combustion, aerodynamics, electromagnetic wave shielding and decontamination.

Isabelle Ribet-Mohamed received an Engineering Diploma from the Ecole Superieure d'Optique, Institut d'Optique, Orsay, France, in 1998 and the Ph.D degree from the University of Paris XI, France, in 2001. Since 2001, she has been a Research Scientist at Onera, Palaiseau, France. Her current research deals with infrared detectors.